arXiv:hep-ph/9501268v2 29 Sep 1995

(revised version of hep-ph/9501268, DO-TH-94/20, THES-TP-94/06)
September 1995

Condensation effects beyond one loop in the Top-mode Standard Model without gauge bosons

G. Cvetič and **E.A. Paschos**
Inst. für Physik, Universität Dortmund, 44221 Dortmund, Germany

N.D. Vlachos
Dept. of Theor. Physics, Aristotle University of Thessaloniki, 540 06 Thessaloniki, Greece

Abstract

We study dynamical symmetry breaking in the Standard Model including the next-to-leading order terms. We introduce at a high, but finite, energy scale Λ a top quark condensate $H = \langle t\bar{t} \rangle$ and derive, using path integral methods, the effective potential including quadratic fluctuations in the scalar field H. We neglect the contributions of all components of the massive electroweak gauge bosons. The existence of a non-trivial minimum in the effective potential leads to the condition that the cut-off Λ is limited from above: $\Lambda \stackrel{<}{\approx} \Lambda_{\rm crit} \approx 4.7 m_t^{\rm phys.}$ (for $N_{\rm c} = 3$), and to a new lower bound for the 4-fermion coupling $a = (G N_{\rm c} \Lambda^2)/(8\pi^2) \stackrel{>}{\approx} 1.60$. Similar results are obtained if we demand, instead, that the next-to-leading order contributions not shift the location $z = (m_{\rm t}^{\rm bare}/\Lambda)^2$ of the minimum drastically, e.g. by not more than a factor of 2. The results are reproduced diagrammatically, where the leading plus all the next-to-leading order diagrams in the $1/N_{\rm c}$-expansion are included. Dominant QCD effects are also included, but their impact on the numerical results is shown to be small.

PACS number(s): 11.15.Pg, 12.50.Lr

1 Introduction

Inspired by the pioneering work of Nambu and Jona-Lasinio (NJL) [1], many studies appeared in the past which consider the Higgs mesons as bound states (condensates) of heavy quark pairs ([2]-[6] and references therein) . Usually, the 1-loop effective potential of the Higgs condensate is calculated starting with effective 4-fermion interactions, whose origin is a new as yet unknown physics at higher energies. While the Higgs field is assumed to be auxiliary (non-dynamical) at the outset, it becomes dynamical through (1-loop) quantum effects. In order to investigate qualitative features of condensation and to avoid additional technical difficulties, the calculation is frequently performed by ignoring the effects of the electroweak gauge bosons and taking into account only the effects of fermionic loops - this is frequently called the large-$N_{\rm c}$ approximation. The vacuum expectation value (VEV) is the value of the Higgs field at the minimum of the effective potential. This condition is a relation between the mass of the heavy quark (usually the top quark), the 4-fermion coupling parameters and the energy cut-off Λ where the condensation occurs. The relation is called the 1-loop gap equation.

The dynamical symmetry breaking (DSB), as manifested by the condensation, is essentially a non-perturbative phenomenon. Nonetheless, the effective potential can be calculated perturbatively. At 1-loop level, the summation of an infinite number of the relevant diagrams, for any fixed value of the internal 4-momentum $\bar{k}$, leads to an analytic function which gives naturally the analytic continuation into regions of low energy ($\bar{k}^2 < m_t^2$) where the original perturbative series does not converge [10]. These analytic functions can be subsequently integrated over the internal momenta $\bar{k}$, incorporating in this way the non-perturbative regions.

Here we emphasize that we consider the effective potential as a function of only a hard mass term $\lambda\sigma_0$ of the top quark, parametrized by the expectation value σ_0 of a composite (initially auxiliary) scalar field σ. On the other hand, we note that there exists a more general formalism for the DSB developed by Cornwall, Jackiw and Tomboulis [7], which is variational and studies the general functional form $\Sigma(\not{p})$ of the expectation value of the proper self-energy part in the quark propagator.

In this article, we derive the effective potential $V_{\rm eff}$ beyond the one loop by the path integral method, and later on we reproduce the results diagrammatically, summing up the leading plus the next-to-leading order diagrams in the $1/N_{\rm c}$-expansion. We work within the framework of the NJL-inspired Top-mode Standard Model (TSM) [4] and neglect the effects of all components of the electroweak (massive) gauge bosons. Although path integral methods are to a certain extent known in the literature of the NJL-type models (cf. [8] and references therein), we decided, for reasons of clarity, to present in Section 2 a comprehensive derivation of the effective potential $V_{\rm eff}$ using these methods. We include there the contribution of $V_{\rm eff}^{\rm (ntl)}$ produced by quadratic quantum fluctuations of the Higgs condensate around its "classical" value H_0. Technical details of this calculation are given in Appendices A and B. In Appendix C, we rederive $V_{\rm eff}^{\rm (ntl)}$ diagrammatically and demonstrate that it represents the contributions of all those $(\ell+1)$-loop diagrams ($\ell = 1,2,3,\ldots$) which are next-to-leading order ($\mathcal{O}(1)$) in the formal $1/N_{\rm c}$-expansion[1]. We then calculate in Section 3 the dominant part of the QCD contributions to $V_{\rm eff}$ using the diagrammatic method and demonstrate that their numerical impact is small. In Section 4 we investigate the minimum of $V_{\rm eff}$ and arrive at an improved gap equation – an improved relation between m_t, Λ and the 4-fermion coupling parameter G. The requirement of the existence of a non-trivial minimum (non-zero VEV) in $V_{\rm eff}$ leads to an additional restriction (upper bound) on the value of the physically interesting parameter Λ/m_t. We demonstrate explicitly that the existence of a non-trivial minimum of the effective potential, within the present framework, implies an upper bound for Λ/m_t of $\mathcal{O}(10^1)$. Similar results are obtained when the requirement of the existence of the minimum is replaced by the requirement that the next-to-leading order contributions, discussed in this paper, not shift the location of the minimum drastically. Consequently, the energy Λ, where the top and antitop condense to form the Higgs, cannot be very high. Within the present framework we discuss in Section 5 renormalization corrections to the mass m_t. The new result of the present analysis is an upper bound for Λ of the order of TeV, which is absent in previous studies of Top-mode Standard Model using the 1-loop gap equation.

2 Calculation of the effective potential beyond one loop - contributions of the scalar sector

The Top-mode Standard Model (TSM) [4] is a framework with a truncated gauge-invariant 4-fermion interaction at a high energy scale $E \sim \Lambda$

$$\mathcal{L} = \mathcal{L}^0_{\rm kin} + G\left(\bar{\Psi}^{ia}_{\rm L} t_{{\rm R}a}\right)\left(\bar{t}^b_{\rm R}\Psi^i_{{\rm L}b}\right) \qquad \text{for } E \sim \Lambda \ , \tag{1}$$

where the color indices (a,b) are summed over, $\Psi^T_{\rm L} = (t_{\rm L}, b_{\rm L})$, and $\mathcal{L}^0_{\rm kin}$ represents the familiar gauge-invariant kinetic terms of fermions and gauge bosons. The Lagrangian (1) can be rewritten in terms of an as yet auxiliary scalar field H

$$\mathcal{L} = i\bar{\Psi}^a \partial\!\!\!/ \Psi_a - \frac{1}{\sqrt{2}} M_0 \sqrt{G} H \bar{t}^a t_a - \frac{1}{2} M_0^2 H^2 \ , \tag{2}$$

where H is the real lower component of an auxiliary complex isodoublet field Φ, and M_0 is the bare mass of the field H (at Λ). This field becomes a physical Higgs through quantum effects. We consider this as a prototype model and do not include electroweak gauge bosons. Furthermore, we do not include in (2) the remaining degrees of freedom of the Higgs isodoublet Φ – they represent (after the condensation) the non-physical Goldstones which are gauged away into the longitudinal parts of the gauge bosons in the unitary gauge[2]. In a more realistic framework, we should include either Goldstone bosons or the entire massive electroweak vector bosons. This enlarged problem requires new computational methods and has not been solved yet. We are presently studying the next-to-leading order corrections from Goldstone bosons and hope to present their impact in the future. We have also studied modifications from QCD, which are described in Section 3.

---

[1] The superscript "ntl" stands throughout the paper for the *next-to-leading* order in the $1/N_{\rm c}$-expansion. The $V^{(1)}_{\rm eff}$, originating from the 1-loop 1-PI diagrams, represents at the same time all the *leading* order ($\mathcal{O}(N_{\rm c})$) contributions to $V_{\rm eff}$ in the $1/N_{\rm c}$-expansion.

We simplify the notation by defining

$$\sigma = \frac{M_0}{\sqrt{2}} H \ , \quad \lambda = \sqrt{G} \quad \Longrightarrow \quad \mathcal{L} = i\bar{\Psi}^a \partial\!\!\!/ \Psi_a - \lambda \sigma \bar{t}^a t_a - \sigma^2 \ . \tag{3}$$

The effective potential is the energy density of the ground state when the order parameter $\sigma_0 = \langle \sigma \rangle$ is kept fixed. In the path integral formulation, this condition is incorporated by inserting a δ-function in the generating functional for the Lagrangian [8], [9]

$$\exp\left[-\frac{i}{\hbar} \Omega V_{\text{eff}}(\sigma_0) \right] = Z_0^{-1} \int \mathcal{D}\sigma \int \mathcal{D}\bar{\Psi}\mathcal{D}\Psi \delta \left[\int \left(\sigma(x) - \sigma_0 \right) d^4x \right] \exp\left[\frac{i}{\hbar} \int \mathcal{L} d^4x \right] \ , \tag{4}$$

where Ω is the 4-dimensional volume (formally infinite) and σ_0 is a constant value of the $\sigma(x)$-field. In the generating functional Z_0, mentioned above,

$$Z_0 = \int \mathcal{D}\sigma \int \mathcal{D}\bar{\Psi}\mathcal{D}\Psi \exp\left[\frac{i}{\hbar} \int \mathcal{L} d^4x \right] \tag{5}$$

appears the Lagrangian of eq. (2), and is independent of σ_0. The δ-function can be written in its exponential form

$$\delta(\theta) = (2\pi)^{-1} \int_{-\infty}^{+\infty} dJ e^{-i\theta J} \ , \qquad \text{where:} \ \ \theta = \int d^4x (\sigma(x) - \sigma_0) \ , \tag{6}$$

which brings the fields σ and σ_0 to the exponential. Then, going to the Euclidean space by performing Wick's rotation ($id^4x \mapsto d^4\bar{x}$) and using the units in which $\hbar = 1$, we rewrite (4)

$$\begin{aligned} \exp[-\Omega V_{\text{eff}}(\sigma_0)] = & \ \text{const} \times \int_{-\infty}^{+\infty} dJ \int \mathcal{D}\sigma \int \mathcal{D}\bar{\Psi}\mathcal{D}\Psi \times \\ & \times \exp\left\{ - \int d^4\bar{x} \left[-i\bar{\Psi}^a \bar{\partial\!\!\!/} \Psi_a + \lambda \sigma(\bar{x}) \bar{t}^a t_a + \sigma(\bar{x})^2 + iJ \left(\sigma(\bar{x}) - \sigma_0 \right) \right] \right\} \ . \end{aligned} \tag{7}$$

---

[2] Stated otherwise, we will be looking only at the effects of the purely scalar part ($(G/4)\bar{t}^a t_a \bar{t}^b t_b$) of the 4-fermion interaction (1). Only this part is responsible, within the present framework where the effects of the loops of (massive) electroweak gauge bosons are neglected, for the condensation of a $\bar{t}t$-pair into a scalar Higgs H.

The bars over space-time components and over derivatives indicate the Euclidean quantities [3] , Ω is the Euclidean 4-dimensional volume, "const" is a σ_0-independent quantity. Note that $\bar{\not\partial} = \not\partial$ ($\bar{\gamma}^0 = i\gamma^0, \bar{\gamma}^j = \gamma^j$). The form (7) is convenient for Gaussian integrations. We integrate out the fermionic degrees of freedom

$$\int \mathcal{D}\bar{\Psi}\mathcal{D}\Psi \exp\left\{-\int d^4\bar{x}\left[-i\bar{\Psi}^a \bar{\not\partial}\Psi_a + \lambda\sigma\bar{t}^a t_a\right]\right\} = \det\hat{B}[\sigma] = \exp\left\{Tr\ln\hat{B}[\sigma]\right\} \ , \tag{8}$$

where the operator $\hat{B}$ is defined by its matrix element in the $\bar{x}$-basis

$$\left\langle \bar{x'}; j, a|\hat{B}[\sigma]|\bar{x}; k, b\right\rangle = \delta_{jk}\delta_{ab}\left[i\bar{\gamma}^\mu \frac{\partial}{\partial\bar{x}^\mu} + \lambda\sigma(\bar{x})\delta_{j1}\right]\delta^{(4)}(\bar{x} - \bar{x'}) \ , \tag{9}$$

the indices j, k $(= 1, 2)$ being the isospin and a, b $(= 1, 2, 3)$ the color indices. We are searching for the effective potential at values σ_0 of the scalar field close to the minimum. Fluctuations around this clasical value σ_0 are denoted by $\sigma_1(\bar{x})$, which, of course, must be small

$$\sigma(\bar{x}) = \sigma_0 + \sigma_1(\bar{x}) \ , \qquad \left(\sigma_0 = \frac{M_0}{\sqrt{2}} H_0\right) \ . \tag{10}$$

We can now perform in (8) the expansion in powers of $\sigma_1(\bar{x})$

$$\begin{aligned} \ln\hat{B}[\sigma] &= \ln\hat{B}[\sigma_0] + \ln\left[1 + \lambda\delta_{j1}\hat{B}[\sigma_0]^{-1}\hat{\sigma}_1\right] \\ &= \ln\hat{B}[\sigma_0] + \delta_{j1}\left\{\lambda\hat{B}[\sigma_0]^{-1}\hat{\sigma}_1 - \frac{1}{2}\lambda^2\left(\hat{B}[\sigma_0]^{-1}\hat{\sigma}_1\right)^2 + \cdots\right\} \ . \end{aligned} \tag{11}$$

Here, the dots represent quantum fluctuations of higher order than quadratic. The $\hat{\sigma}_1$-operator is defined through: $\langle\bar{x'}|\hat{\sigma}_1|\bar{x}\rangle = \sigma_1(\bar{x})\delta^{(4)}(\bar{x} - \bar{x'})$. The terms linear in σ_1 do not contribute to $V_{\text{eff}}(\sigma_0)$, due to the δ-function in (4). Hence, eqs. (7)-(11) yield

$$\begin{aligned} \exp[-\Omega V_{\text{eff}}(\sigma_0)] = {} & \text{const} \times \exp\left\{-\int d^4\bar{x}[\sigma_0^2] + Tr\ln\hat{B}[\sigma_0]\right\} \times \\ & \times \int_{-\infty}^{+\infty} dJ \int \mathcal{D}\sigma_1 \exp\left\{-\int d^4\bar{x}\sigma_1(\bar{x})^2 - \frac{1}{2}\lambda^2 Tr\left[(\hat{B}[\sigma_0]^{-1}\hat{\sigma}_1)^2\right] - J\int d^4\bar{x}\sigma_1(\bar{x})\right\} \ , \end{aligned} \tag{12}$$

where we neglected the effects of cubic and higher quantum fluctuations. The first factor in (12) gives us the usual tree level and 1-loop contribution to V_{eff}

$$(V_{\text{eff}}^{(0)} + V_{\text{eff}}^{(1)})(\sigma_0) = \sigma_0^2 - \frac{1}{\Omega} Tr\ln\hat{B}[\sigma_0] = \sigma_0^2 - \frac{N_{\text{c}}}{(2\pi)^4} tr_{\text{f}} \int d^4\bar{k}\ln(\bar{\gamma^\mu}\bar{k^\mu} + \lambda\sigma_0) \ . \tag{13}$$

The integral on the r.h.s. is derived in Appendix A. The factor N_{c} comes from the trace over colors, and the remaining tr_{f} denotes tracing in the 4-dimensional spinor space. By expanding the logarithm in (13) in powers of $[\lambda\sigma_0(\bar{\gamma^\mu}\bar{k^\mu})^{-1}]$, we obtain

---

[3] Factor i survives at J in the exponent in (7). This is so because the δ-function constraint, which excludes the contributions of the constant modes of $\sigma - \sigma_0$, must remain valid also in the Euclidean metric.

$$(V_{\mathrm{eff}}^{(0)} + V_{\mathrm{eff}}^{(1)})(\sigma_0) = \sigma_0^2 - \frac{N_{\mathrm{c}}}{(8\pi^2)} \int_0^\infty d\bar{k}^2 \bar{k}^2 \ln \left[1 + \frac{\lambda^2 \sigma_0^2}{\bar{k}^2} \right] \ . \tag{14}$$

The expression (14) can also be obtained by calculating the relevant 1-PI diagrams with one loop of the top quark and zero momentum Higgs particles as the outside legs. This calculation is described, for example, in ref. [10] where the notation of eq. (2) was used.

To go beyond one loop, we must integrate the path integral in (12) containing the quantum fluctuations σ_1^2 and $J\sigma_1$ of the scalar in the exponent. This can be done, by using known formulas for path integrals of Gaussian distributions (e.g. ref. [11]). We consider the general expression

$$\begin{aligned} \int \mathcal{D}\sigma_1 \exp \left\{ -\frac{1}{2} \int d^4\bar{x} d^4\bar{x'} \sigma_1(\bar{x'}) \hat{A}(\bar{x'}, \bar{x}) \sigma_1(\bar{x}) - iJ \int d^4\bar{x} \sigma_1(\bar{x}) \right\} = \\ \exp \left[-\frac{1}{2} Tr \ln \hat{A} \right] \exp \left[-\frac{1}{2} J^2 \int d^4\bar{x} d^4\bar{x'} \hat{A}^{-1}(\bar{x'}, \bar{x}) \right] \ , \end{aligned} \tag{15}$$

where [4] for our case

$$\hat{A}(\bar{x'}, \bar{x}) = 2\delta(\bar{x'} - \bar{x}) + \lambda^2 tr \Big\{ \langle \bar{x} | \hat{B}[\sigma_0]^{-1} | \bar{x'} \rangle \langle \bar{x'} | \hat{B}[\sigma_0]^{-1} | \bar{x} \rangle \Big\} \ , \tag{16}$$

as inferred from (12). Here, *tr* stands for the trace over the color, isospin and spinor degrees of freedom.

Furthermore, the integration over J in (12) of the exponential factor containing J^2 of (15) (i.e., the effect of the δ-function) can also be explicitly performed

$$\int_{-\infty}^{+\infty} dJ \exp \left[-\frac{1}{2} J^2 \int d^4\bar{x} d^4\bar{x'} \hat{A}^{-1}(\bar{x'}, \bar{x}) \right] = \sqrt{\frac{2\pi}{\alpha}} \ , \tag{17}$$

$$\text{where} \qquad \alpha = \int d^4\bar{x} d^4\bar{x'} \hat{A}^{-1}(\bar{x'}, \bar{x}) = \frac{\Omega}{\tilde{A}(\bar{p} = 0)} \ . \tag{18}$$

We note that $\alpha > 0$ for all interesting regions of values of $\lambda\sigma_0$ (see Appendix B), hence the integral in (17) is convergent. We obtain from (12), (15)-(18) for the contribution of quadratic fluctuations to the effective potential the following expression

$$V_{\mathrm{eff}}^{(\mathrm{ntl})}(\sigma_0) = \frac{1}{2\Omega} Tr \ln \hat{A} - \frac{1}{2\Omega} \ln \left[\tilde{A} \left(\bar{p} = 0, \lambda^2 \sigma_0^2 \right) \right] + \cdots \ , \tag{19}$$

---

[4] Formula (15) can be obtained from its well-known special case of $J = 0$ by a simple substitution of variables: $\hat{\sigma}_1 \mapsto \hat{\sigma}_1 - iJ\hat{A}^{-1}$. Furthermore, an identity has to be used whose 1-dimensional analogue reads: $\int_{-\infty}^{+\infty} dz \exp[-z^2] = \int_{-\infty}^{+\infty} exp[-(z + iy)^2]$, where y is any real constant. This identity applies also in our case, because $\hat{A}$ and $\hat{A}^{-1}$ are symmetric and real in the $\bar{x}$-basis, as shown in Appendix A and this Section.

where the superscript "ntl" stands for the "next-to-leading" order (beyond one loop) and the dots represent irrelevant σ_0-independent terms. The first term on the r.h.s. of eq. (19) is Ω-independent in the limit Ω $(= \int d^4\bar{x}) \to \infty$ (see below). $\tilde{A}(\bar{p})$ in the second term will be calculated below, with a finite energy cut-off Λ, and this integral is finite. Thus the second term goes to zero as $\Omega \to \infty$. Hence, this term, which originates from the δ-function of the path integral (4), drops out. The δ-function in the path integral (4) turns out to have the *sole* effect of ensuring that the quantum fluctuations linear in $\sigma_1(\bar{x})$ do not contribute to the effective potential.

The tracing in $Tr \ln \hat{A}$ can be performed in the momentum basis. For this we need the Fourier transform $\tilde{A}(\bar{p})$ of the operator $\hat{A}$ (see Appendix A for details)

$$\langle \bar{x'} | \hat{A} | \bar{x} \rangle = \hat{A}(\bar{x'}, \bar{x}) = (2\pi)^{-4} \int d^4\bar{p} e^{i\bar{p}(\bar{x} - \bar{x'})} \tilde{A}(\bar{p}) \ , \qquad \tilde{A}(\bar{p}) = 2[1 - 2\lambda^2 N_{\mathrm{c}} \mathcal{K}_H(\bar{p}^2, \lambda^2\sigma_0^2)] \ ,$$

$$\mathcal{K}_H(\bar{p}^2, \lambda^2\sigma_0^2) = \frac{1}{4} \int_{\bar{k}^2 \leq \Lambda_{\mathrm{f}}^2} \frac{d^4\bar{k}}{(2\pi)^4} tr_{\mathrm{f}} \left[\frac{i}{(\bar{\not{k}} - \lambda\sigma_0)} \frac{i}{(\bar{\not{p}} + \bar{\not{k}} - \lambda\sigma_0)} \right] \ . \tag{20}$$

The integral over $\bar{k}$ would be in general over an infinite volume. However, at the $t\bar{t}$-condensation scale $E \sim \Lambda$ we expect that a new dynamics cuts off the integral. We stress that we are working all the time in an effective theory of eq. (1), i.e., in the TSM. For this reason, we introduced in the above integral an energy cut-off Λ_{f} for the fermionic (top quark) Euclidean mometum $\bar{k}$. For simplicity, the cut-off was chosen to be spherical. This Λ_{f} is to be recognized as being approximately the energy Λ of (1) at which the $\bar{t}t$-condensation takes place. Similarly, the tracing in $Tr \ln \hat{A}$ in the momentum basis involves a second integral – over the bosonic (Higgs) momenta $\bar{p}$. By the arguments just discussed, we introduce for these momenta a second spherical cut-off Λ_{b}, where $\Lambda_{\mathrm{b}} \sim \Lambda$. The tracing in $Tr \ln \hat{A}$ in the momentum basis is performed in Appendix A, by using the expression (20). Then we rescale all the Euclidean 4-momenta $\{\bar{k}^2, \bar{p}^2\} \mapsto \Lambda_{\mathrm{f}}^2 \{\bar{k}^2, \bar{p}^2\}$ and end up with the following result

$$V_{\mathrm{eff}}^{(\mathrm{ntl})}(\sigma_0) = \frac{\Lambda_{\mathrm{f}}^4}{2(4\pi)^2} \int_0^{\Lambda_{\mathrm{b}}^2/\Lambda_{\mathrm{f}}^2} d\bar{p}^2 \bar{p}^2 \ln \left[1 - a \mathcal{J}_H(\bar{p}^2, \varepsilon^2) \right] \ , \tag{21}$$

$$\text{where we denote:} \qquad \varepsilon^2 = \frac{\lambda^2}{\Lambda_{\mathrm{f}}^2} \sigma_0^2 = \frac{G M_0^2}{2\Lambda_{\mathrm{f}}^2} H_0^2 \ , \qquad a = \frac{(G N_{\mathrm{c}} \Lambda_{\mathrm{f}}^2)}{(8\pi^2)} \ ,$$

$$\text{and:} \qquad \mathcal{J}_H(\bar{p}^2, \varepsilon^2) = \frac{16\pi^2}{\Lambda_{\mathrm{f}}^2} \mathcal{K}_H(\Lambda_{\mathrm{f}}^2 \bar{p}^2, \lambda^2\sigma_0^2) = (\pi)^{-2} \int_{\bar{k}^2 \leq 1} d^4\bar{k} \frac{[\bar{k}(\bar{p} + \bar{k}) - \varepsilon^2]}{(\bar{k}^2 + \varepsilon^2)[(\bar{p} + \bar{k})^2 + \varepsilon^2]} \ . \tag{22}$$

This is the main result of the analysis so far, giving a closed form of the next-to-leading effective potential. As just argued, we expect: $\Lambda_{\mathrm{f}} \sim \Lambda_{\mathrm{b}} \sim \Lambda$, where Λ is from (1). Our numerical results depend on the ratio $\Lambda_{\mathrm{b}}/\Lambda_{\mathrm{f}}$. However, since we are interested primarily in the qualitative features of the next-to-leading order corrections, we will assume the equality of the two cut-offs

$$\Lambda_{\mathrm{f}} = \Lambda_{\mathrm{b}} = \Lambda \ . \tag{23}$$

The parameter a in (21) can be easily expressed through the ratio $z_1 = (m_t^{(1)}/\Lambda)^2$, $m_t^{(1)}$ being the solution of the 1-loop gap equation for the mass of the top quark. The 1-loop gap equation follows from

$$\frac{\partial}{\partial \varepsilon^2}\left(V_{\mathrm{eff}}^{(0)} + V_{\mathrm{eff}}^{(1)}\right)\Big|_{\varepsilon^2 = z_1} = 0 \ , \qquad \text{which gives}$$

$$a = \frac{G N_{\mathrm{c}} \Lambda^2}{(8\pi^2)} = [1 - z_1 \ln(z_1^{-1} + 1)]^{-1} \ (= \mathcal{O}(1)) \ , \qquad \text{where: } z_1 = \left(\frac{m_t^{(1)}}{\Lambda}\right)^2 \ . \tag{24}$$

The newly introduced dimensionless parameter a is $\mathcal{O}(1)$ ($a > 1$). Furthermore, the integral $\mathcal{J}_H(\bar{p}^2, \varepsilon^2)$ can be integrated analytically (see Appendix B). The effective potential has the following terms

$$\begin{aligned} V_{\mathrm{eff}}(\varepsilon^2) &= (V_{\mathrm{eff}}^{(0)} + V_{\mathrm{eff}}^{(1)} + V_{\mathrm{eff}}^{(\mathrm{ntl})})(\varepsilon^2) \\ &= \left(\frac{N_{\mathrm{c}} \Lambda^4}{8\pi^2}\right)\left\{\frac{\varepsilon^2}{a} - \int_0^1 d\bar{p}^2 \bar{p}^2 \ln(1 + \frac{\varepsilon^2}{\bar{p}^2}) + \frac{1}{4N_{\mathrm{c}}}\int_0^1 d\bar{p}^2 \bar{p}^2 \ln\left[1 - a\mathcal{J}_H(\bar{p}^2, \varepsilon^2)\right]\right\} \ . \end{aligned} \tag{25}$$

It is now evident that $V_{\mathrm{eff}}^{(\mathrm{ntl})}$ is next-to-leading order in the $1/N_{\mathrm{c}}$-expansion.

The effective potential can also be derived by the diagrammatic method. The derivation of $V_{\mathrm{eff}}^{(1)}$ is described, for example, in ref. [10]. The new term $V_{\mathrm{eff}}^{(\mathrm{ntl})}$ is derived in Appendix C. The relevant diagrams turn out to be those shown in Fig. 3. It is also shown in the Appendix that the diagrams of Fig. 3 are all of $\mathcal{O}(1)$ in the $1/N_{\mathrm{c}}$-expansion, and that there are no other contributing diagrams of $\mathcal{O}(1)$. An important feature is the fact that each top quark loop involves an arbitrary number of external scalar lines with zero momenta. The $(a\mathcal{J}_H)^{\ell}$-term in the expansion of the last logarithm in (25) is in fact the contribution of the $(\ell + 1)$-loop diagram of Fig. 3. For example, the first element in this expansion, $(a\mathcal{J}_H)^1$, is the self-energy of the scalar particle from the top quark loop, joined together in a closed ring – the 2-loop version of Fig. 3. From this Figure, it becomes evident why we have identified in (20) the Euclidean 4-momentum $\bar{k}$ as the fermionic (top quark) momentum with a cut-off Λ_{f}, and $\bar{p}$ as the bosonic (Higgs) momentum with a cut-off Λ_{b}.

Finally, we emphasize that the diagrammatic method involves tedious combinatorics and summations. However, its pictorial transparency makes it possible to adapt it easily to other interactions, like the QCD interaction between the gluon and the top quark. The latter results in contributions of QCD to the effective potential, which are studied in the nect Section.

3 QCD contributions to the effective potential

As mentioned already, the dominant part of the gluonic contributions to V_{eff} can be calculated in a straightforward way by a generalization of the diagrammatic method, in complete analogy to the calculation presented in Appendix C for the contribution of the Higgs sector to $V_{\rm eff}$. The relevant graphs are those of Fig. 3, where now all the internal dotted lines represent a gluon of a specific color. The results (C.7)-(C.10) can basically be transcribed, if we simply replace the "Yukawa" coupling $\sqrt{G}M_0/\sqrt{2} \mapsto g_{\rm s}\lambda^a\gamma_\mu/2$ (where: $g_{\rm s}^2/(4\pi) = \alpha_{\rm s}$; $\lambda^a/2$ are the generators of the $SU(3)_c$-group). In addition, we replace the non-dynamical Higgs propagator $(-i)/M_0^2$ by the gluon propagator $(-i)\delta^{ab}\left(g^{\mu\nu} - p^\mu p^\nu/p^2\right)/p^2$ (a, b are color indices). For the gluons we use the Landau gauge, in which there is no (1-loop) QCD contribution to the quark wave function renormalization. In close analogy to Appendix C, we obtain for the contribution of the gluonic diagrams (in the Eucl. metric)

$$V_{\rm eff}^{(\rm gl)}(\sigma_0) = \frac{1}{2(4\pi)^2}(N_{\rm c}^2-1)\int_0^{\Lambda_{\rm b}^2} d\bar{p}^2\bar{p}^2 \ln\left[1 - 2g_{\rm s}^2\mathcal{K}_{\rm gl}\left(\bar{p}^2,\lambda^2\sigma_0^2\right)\right] \ , \tag{26}$$

$$\begin{aligned}\text{where:}\quad \mathcal{K}_{\rm gl}\left(\bar{p}^2,\lambda^2\sigma_0^2\right) &= \mathcal{K}^{\mu\nu}\left(\bar{p}^2,\lambda^2\sigma_0^2\right)\frac{1}{\bar{p}^2}\left(\delta^{\mu\nu} - \frac{\bar{p}^\mu\bar{p}^\nu}{\bar{p}^2}\right) \ , \\ \mathcal{K}^{\mu\nu}\left(\bar{p}^2,\lambda^2\sigma_0^2\right) &= \frac{1}{4}\int\frac{d^4\bar{k}}{(2\pi)^4}tr_{\rm f}\left[\bar{\gamma}^\mu\frac{i}{\left(\bar{\not{k}} - \lambda\sigma_0\right)}\bar{\gamma}^\nu\frac{i}{\left(\bar{\not{p}} + \bar{\not{k}} - \lambda\sigma_0\right)}\right] \ .\end{aligned} \tag{27}$$

We point out that the contributions of those diagrams of Fig. 3 which contain simultaneously scalar and gluonic internal propagators are zero. This is so because in such diagrams there is at least one top quark loop which has one scalar and one gluon propagator attached to it, thus resulting in a factor proportional to the trace over colors $tr(\lambda^a) = 0$.

The integral over the top quark momentum in $\mathcal{K}^{\mu\nu}$ can be regularized by several methods, provided they respect the symmetries of the QCD gauge theory (Lorentz invariance, etc.). QCD being a renormalisable theory, the self-energy of the gluons, and thus $\mathcal{K}^{\mu\nu}$, have only logarithmic cut-off dependence. This is in strong contrast with the scalar sector, which has Λ^2-terms under any regularization - cf. eq. (20). The integral for $\mathcal{K}^{\mu\nu}$ thus obtained is well-known in the literature. Using the well-known technique of exponentiating the denominators as integrals of exponentials, it can be written in the "proper time" form (and in Euclidean metric)

$$\mathcal{K}^{\mu\nu}\left(\bar{p}^2,\lambda^2\sigma_0^2\right) = \frac{\left(-\delta^{\mu\nu}\bar{p}^2 + \bar{p}^\mu\bar{p}^\nu\right)}{8\pi^2}\int_0^1 dz z(1-z)\int_0^\infty\frac{d\tau}{\tau}\rho_{\rm f}(\tau;\Lambda_{\rm f})\exp\left\{-\tau\left[z(1-z)\bar{p}^2 + \lambda^2\sigma_0^2\right]\right\} \ , \tag{28}$$

where $\rho_{\rm f}(\tau;\Lambda_{\rm f})$ is a regulator for the fermionic (top quark) momenta, with some effective cut-off $\Lambda_{\rm f}$. Note that $\rho_{\rm f} = 1$ for $\tau \gg 1/\Lambda$, and $\rho_{\rm f} = 0$ for $\tau \ll 1/\Lambda$. The regulator eliminates the $\Lambda_{\rm f}^2$-term in $\mathcal{K}^{\mu\nu}$. Among the many choices, we select two different regulators $\rho_{\rm f}$: the simple Pauli-Villars (P.V.) subtraction; and the "proper time" cut-off ($\rho_{\rm f}(\tau;\Lambda_{\rm f}) = \theta(\tau - 1/\Lambda_{\rm f}^2)$)

$$\mathcal{K}^{\mu\nu}_{\rm P.V.}\left(\bar{p}^2,\lambda^2\sigma_0^2\right) = \mathcal{K}^{\mu\nu}\left(\bar{p}^2,\lambda^2\sigma_0^2\right) - \mathcal{K}^{\mu\nu}\left(\bar{p}^2,\Lambda_{\rm f}^2\right) \ , \tag{29}$$

$$\mathcal{K}^{\mu\nu}_{\text{p.t.}}\left(\bar{p}^2, \lambda^2\sigma_0^2\right) = \frac{1}{8\pi^2}\left(-\delta^{\mu\nu}\bar{p}^2 + \bar{p}^\mu\bar{p}^\nu\right)\int_0^1 dz z(1-z)\int_{1/\Lambda_{\text{f}}^2}^{\infty}\frac{d\tau}{\tau}\exp\left\{-\tau\left[z(1-z)\bar{p}^2 + \lambda^2\sigma_0^2\right]\right\} . \quad (30)$$

Both of these integrals can be integrated analytically. This then leads to the following dominant part of the gluonic contributions [5] to V_{eff}

$$V_{\text{eff}}^{(\text{gl})}\left(\varepsilon^2\right) = \frac{\Lambda^4}{2(4\pi)^2}\left(N_{\text{c}}^2 - 1\right)\int_0^1 d\bar{p}^2\bar{p}^2\ln\left[1 - a_{\text{gl}}\mathcal{J}_{\text{gl}}\left(\bar{p}^2, \varepsilon^2\right)\right] , \quad (31)$$

$$\begin{aligned}
\text{where:} \quad \mathcal{J}_{\text{gl}}\left(\bar{p}^2, \varepsilon^2\right) &= \frac{8\pi^2}{3}\mathcal{K}_{\text{gl}}\left(\Lambda^2\bar{p}^2, \lambda^2\sigma_0^2 = \Lambda^2\varepsilon^2\right) , \\
a_{\text{gl}} &= \frac{3}{4\pi^2}g^2_{\text{s}} = \frac{3\alpha_{\text{s}}}{\pi} \approx 0.105 \qquad (\text{for } \alpha_{\text{s}} = \alpha_{\text{s}}(m_t) \approx 0.11) . \quad (32)
\end{aligned}$$

The explicit expressions for J_{gl} for the case of one simple Pauli-Villars subtraction and for the case of the "proper time" cut-off are given at the end of Appendix B (see eqs. (B.11) and (B.12)). The expression (31) represents in a sense the "leading-logarithmic" QCD contribution to V_{eff}. Evidently, it includes the two loop contribution, represented by the following simple diagram integrated over the quark and gluon momenta: $\bar{t}t$-loop and a gluon propagator across it (2-loop version of Fig. 3). This leading two-loop contribution of QCD to V_{eff} is obtained from (31) by replacing $\ln\left[1 - a_{\text{gl}}\mathcal{J}_{\text{gl}}\left(\bar{p}^2, \varepsilon^2\right)\right]$ by its leading term $\left[-a_{\text{gl}}\mathcal{J}_{\text{gl}}\left(\bar{p}^2, \varepsilon^2\right)\right]$.

It is not possible to identify the expression (31) as corresponding to a next-to-leading contribution in the $1/N_{\text{c}}$-expansion of $V_{\text{eff}}/N_{\text{c}}$ in the case of the *formal* limit $N_{\text{c}} \to \infty$. Unlike the expression (21), or the last term in (25), it contains also the factor $(N_{\text{c}}^2 - 1)$, i.e., the number of gluons (cf. also eq. (33) below). It is not clear whether the QCD contributions can be organized in a systematic way into an $1/N_{\text{c}}$-expansion series whose n'th expansion term would have, for example, a factor $(N_{\text{c}}^2-1)/N_{\text{c}}^n$ in front of it. Such a series would probably be for $N_{\text{c}} = 3$ a convergent or at least an asymptotic series, whose first term would be (31). We point out that the $1/N_{\text{c}}$-expansion (with $N_{\text{c}} = 3$) of V_{eff} in the present paper refers to the contributions from the electroweak (or: scalar, Higgs) sector only, i.e., to the contributions corresponding to the diagrams which contain the top quarks and composite scalars, but no gluons. $N_{\text{c}}(= 3)$ represents in this case the number of top quark types contributing in loops separately to the condensation. The related expansion of these contributions in powers of $1/3$ $(= 1/N_{\text{c}})$, as discussed in the previous Section and in Appendix C, should therefore be regarded as independent of a particular structure of QCD and of the number of gluons. On the other hand, what is the most simple way to organize the QCD contributions to V_{eff}, so that they would result in a convergent or at least an asymptotic series? Such a series appears to be the direct loop expansion in powers of α_s. In this context, we point out that expression (31), unlike (21), turns out to be almost equal to the two-loop approximation, i.e., to the first term from the expansion of the logarithm, the difference being only a fraction of a percent. This is connected to the fact that, at the considered scales ($m_t < E < \Lambda$), QCD can be treated perturbatively. The smallness of the couplings α_s (or: $a_{\rm gl}$) at these scales makes the total gluonic contribution $V_{\rm eff}^{\rm gl}$ small despite a relatively large coefficient $N_{\rm c}^2 - 1 = 8$.

---

[5] Just like in Section 2, we equate for simplicity the bosonic and the fermionic cut-offs: $\Lambda_{\text{b}} = \Lambda_{\text{f}} = \Lambda$; and rescale the momenta and the masses ($\bar{q}^2 \mapsto \bar{q}^2/\Lambda^2$; $\varepsilon^2 = \lambda^2\sigma_0^2/\Lambda^2$).

4 Analysis of the improved gap equation

Summarizing the results of the previous sections, we write down the effective potential which includes the (0+1)-loop contributions, the next-to-leading contributions ($V_{\rm eff}^{\rm (ntl)}$) and the dominant gluonic contributions ($V_{\rm eff}^{\rm gl}$)

$$V_{\rm eff}(\varepsilon^2) = \left(V_{\rm eff}^{(0)} + V_{\rm eff}^{(1)} + V_{\rm eff}^{\rm (ntl)} + V_{\rm eff}^{\rm (gl)} \right) (\varepsilon^2)$$

$$\begin{aligned} = \ & \left(\frac{N_{\rm c} \Lambda^4}{8\pi^2} \right) \Big\{ \frac{\varepsilon^2}{a} - \int_0^1 d\bar{p}^2 \bar{p}^2 \ln(1 + \frac{\varepsilon^2}{\bar{p}^2}) + \frac{1}{4N_{\rm c}} \int_0^1 d\bar{p}^2 \bar{p}^2 \ln \left[1 - a \mathcal{J}_H(\bar{p}^2, \varepsilon^2) \right] + \\ & + \frac{(N_{\rm c}^2 - 1)}{4N_{\rm c}} \int_0^1 d\bar{p}^2 \bar{p}^2 \ln \left[1 - a_{\rm gl} \mathcal{J}_{\rm gl}(\bar{p}^2, \varepsilon^2) \right] \Big\} \ . \end{aligned} \tag{33}$$

We obtain an improved gap equation by minimizing this entire effective potential. This gap equation gives us an improved value $z = (m_t/\Lambda)^2$ as a function of the input parameter $(G\Lambda^2)$ $(= 8\pi^2 a/N_{\rm c})$

$$\begin{aligned} & \Big\{ \frac{1}{a} - \int_0^1 \frac{d\bar{p}^2 \bar{p}^2}{\bar{p}^2 + \varepsilon^2} + \frac{1}{4N_{\rm c}} \frac{\partial}{\partial \varepsilon^2} \int_0^1 d\bar{p}^2 \bar{p}^2 \ln \left[1 - a \mathcal{J}_H(\bar{p}^2, \varepsilon^2) \right] + \\ & + \frac{(N_{\rm c}^2 - 1)}{4N_{\rm c}} \frac{\partial}{\partial \varepsilon^2} \int_0^1 d\bar{p}^2 \bar{p}^2 \ln \left[1 - a_{\rm gl} \mathcal{J}_{\rm gl}(\bar{p}^2, \varepsilon^2) \right] \Big\} \Big|_{\varepsilon^2 = z} = 0 \ . \end{aligned} \tag{34}$$

In Appendix B we give analytic expressions for $\mathcal{J}_H(\bar{p}^2, \varepsilon^2)$ and $\partial \mathcal{J}_H(\bar{p}^2, \varepsilon^2)/\partial \varepsilon^2$ (spherical cut-off), as well as for $\mathcal{J}_{\rm gl}(\bar{p}^2, \varepsilon^2)$ and implicitly for $\partial \mathcal{J}_{\rm gl}(\bar{p}^2, \varepsilon^2)/\partial \varepsilon^2$ (for the case of the simple Pauli-Villars subtraction, and for the case of the "proper time" cut-off). Using these expressions in (34), we calculate the integrals numerically (for a given a and for $N_{\rm c} = 3$) and obtain solutions for $\varepsilon^2 = z = (m_t/\Lambda)^2$ as a function of the input parameter a, that is, of the input parameter $G\Lambda^2 = 8\pi^2 a/N_{\rm c}$. The results are tabulated in the third column (with gluonic contributions included) and in the fifth column (without gluonic contributions) of Table 1, and are depicted in Figs. 1a-1e (for specific input values $G\Lambda^2$) as full lines and long-dashed lines, respectively. For gluons we chose the "proper time" cut-off (30). The results for $\sqrt{z} = m_t/\Lambda$ in the third column of Table 1 change mostly by less than 3 percent if we choose for the gluonic contributions the simple Pauli-Villars subtraction (29) instead.

When solving eq. (34) for $z = z(G\Lambda^2)$, we must always check: that the integrands in (34) and (33)) have no singularities near the minimum $\varepsilon^2 \approx z$ and, in addition, that the stationary point $\varepsilon^2 = z$ of $V_{\rm eff}(\varepsilon^2)$ is really a local minimum. The calculations show that there are no singularities for ε^2 lying near the value of z for the minimum of $V_{\rm eff}$ (cf. discussion in Appendix B). Furthermore, the calculations show an interesting phenomenon: as $a = (N_{\rm c} G\Lambda^2)/(8\pi^2)$ decreases beyond a critical value of approximately 1.50 (1.60 without gluons), the local minimum of the effective potential $V_{\rm eff}(\varepsilon^2)$ disappears at a *non-zero* value $\varepsilon^2 = 0.277^2 \approx 0.08$ ($0.309^2 \approx 0.095$ without gluons), i.e., the dynamical symmetry breaking disappears (see Figs. 1d-1e). This is also seen in Table 1 (first, third and fifth column). Hence, the calculations suggest an upper bound on the energy cut-off Λ ($\simeq E_{\rm condensation}$), and this bound is expressed in terms of the bare mass m_t

$$\frac{m_t}{\Lambda} \gtrsim 0.277 \ (0.309) \qquad \Rightarrow \qquad \Lambda \lesssim 3.61 m_t \ (3.24 m_t) \ . \tag{35}$$

Here and for the rest of this paper, the values in parentheses indicate values when the QCD contributions are ignored. At the same time, these numerical results give a lower bound on the 4-fermion coupling G of eq. (1)

$$a = \frac{N_{\rm c} G \Lambda^2}{8\pi^2} \gtrsim a_{\rm crit.} = 1.499 \ (1.597) \ . \tag{36}$$

We note that the 1-loop gap equation (24) gives a much weaker bound on G, and *no* relation analogous to (35)

$$a = \frac{N_{\rm c} G \Lambda^2}{8\pi^2} \gtrsim 1 \ , \qquad \text{and} \qquad \Lambda \leq \infty \ \ (\text{or: } \Lambda \lesssim E_{\rm Planck}) \ .$$

We also note from Table 1 (third column) that, as G goes down to $G_{\rm crit.} \simeq 1.50 \times 8\pi^2/(N_{\rm c}\Lambda^2)$ (for $N_{\rm c} = 3$), the difference between (m_t/Λ) and the 1-loop solution $(m_t^{(1)}/\Lambda)$ becomes as large as 34 percent. We can also take the following point of view: if we require that the calculated corrections beyond 1-loop do not change the solution $z_1 = (m_t^{(1)}/\Lambda)^2$ of the 1-loop gap equation drastically [6], e.g. not by more than a factor of 2, we arrive at very similar results to those of eqs. (35)-(36)

$$\frac{z}{z_1} > 0.5 \ \Rightarrow \ \frac{m_t}{\Lambda} \gtrsim 0.299 \ (0.332) \ , \ a \gtrsim 1.506 \ (1.605) \ . \tag{37}$$

Furthermore, singularities (cuts) do occur in $V_{\rm eff}^{\rm (ntl)}$ in the region of small ε^2 ($\varepsilon^2 < 0.25 z_1$, for all $a \geq a_{\rm crit.}$), and the (full) lines in Figs. 1a-1e were not continued into these regions. In these regions, the expression in the logarithm of the integrand for $V_{\text{eff}}^{(\text{ntl})}$ becomes negative (cf. Appendix B for discussion). The loop expansion of $V_{\text{eff}}^{(\text{ntl})}$ (i.e., in powers of $[a\mathcal{J}_H(\bar{p}^2, \varepsilon^2)]$, cf. eqs. (C.9), (C.10)) is a divergent series for such small ε^2. These regions of ε^2 do not represent any problem, since the region of our interest is around the minimum of V_{eff} ($\varepsilon^2 \approx z$) which lies a safe distance away from the singularities, even in the critical case $a \approx 1.50$ ($z \approx 0.277^2$, cf. Figs. 1d-1e). Stated otherwise: as long as we require that the calculated next-to-leading corrections to the 1-loop gap solution z_1 do not change this solution drastically ($e.g., z > 0.3 z_1$), i.e., that the $1/N_{\text{c}}$-expansion of the scalar contributions (for $N_{\text{c}} = 3$) make sense, we do not encounter any singularities near the minimum of $V_{\text{eff}}^{(\text{ntl})}$.

---

[6] It is manifestly apparent from the expression for $V_{\rm eff}$ that the natural parameter that should be regarded as the solution of the gap equation is $z = (m_t/\Lambda)^2$, and not $\sqrt{z} = (m_t/\Lambda)$.

The gluonic contributions $V_{\text{eff}}^{(\text{gl})}$ of eq. (31) do not have any of these problems, because $\mathcal{J}_{\text{gl}}(\bar{p}^2, \varepsilon^2)$ turns out to be negative in the entire region of integration. In addition, this $\mathcal{J}_{\text{gl}}$ is numerically very small, and the corresponding logarithm in (31) is in addition suppressed by the small coupling $a_{\text{gl}} \approx 3\alpha_{\text{s}}(m_t)/\pi \approx 0.105$. The smallness of a_{gl} is connected with the perturbative nature of QCD at our relevant energies $E \overset{>}{\sim} m_t$. Therefore, the contributions of gluons are playing a numerically inferior role when compared to those of the next-to-leading Higgs contributions to the gap equations (cf. Table 1 and eqs. (35)-(36)). A consequence of the relative small gluonic contributions is the fact that the results of this paper are practically the same when $V_{\text{eff}}^{(\text{gl})}$ in (31) is replaced by the 2-loop gluonic contribution, i.e., when we replace $\ln\left[1 - a_{\text{gl}}\mathcal{J}_{\text{gl}}\left(\bar{p}^2, \varepsilon^2\right)\right]$ by its leading term $\left[-a_{\text{gl}}\mathcal{J}_{\text{gl}}\left(\bar{p}^2, \varepsilon^2\right)\right]$. This substitution brings a difference of a fraction of a percent. For the next-to-leading Higgs contributions, $V_{\text{eff}}^{(\text{ntl})}$, the situation is different, the 2-loop approximation of $V_{\text{eff}}^{(\text{ntl})}$ differs notably from the full version of $V_{\text{eff}}^{(\text{ntl})}$ (cf. Figs. 1a-1c, dash-dotted and long-dashed lines). For illustration, in Figs. 1a-c we included also the effective potential calculated up to 1-loop (short-dotted line).

5 Mass renormalization corrections and conclusions

It should be pointed out that the solution for m_t through the gap equation (34) (Table 1, third and fifth column) is not the *physical* mass of the top quark in the present framework, but rather the "bare" mass of the top quark in the effective theory with an energy cut-off Λ:

$$m_t = m_t^{\text{bare}} = m_t(\Lambda) \tag{38}$$

In other words, we have calculated essentially the contribution of the tadpoles to m_t, i.e., the value of the condensate $\langle\bar{\Psi}\Psi\rangle$ – in such a framework, the relation between the condensate and the physical mass has been investigated by Politzer [12]. The physical mass $m_t^{\text{ren.}}$ is calculated, within the present framework, by adding up the diagrams of Figs. 5a-c. The dashed lines represent the (composite) Higgs propagator (this results in the next-to-leading in $1/N_{\rm c}$ correction to m_t due to the scalar sector). In addition, we include the usual 1-loop QCD correction $(\delta m_t)^{\rm QCD}$ which is obtained by the diagram of Fig. 5a, where now the dashed line represents the gluonic propagator. We do not include the QCD effects that are higher than this 1-loop QCD renormalization effect. This is justified, because these higher QCD effects are quite negligible, as suggested also by the mentioned smallness of the function $a_{\rm gl}\mathcal{J}_{\rm gl}(\bar{p}^2, \varepsilon^2)$. The second part of Appendix C contains details of the calculation of these diagrams. This leads to the corrected (renormalized) mass of the top quark (cf. (C.14)-(C.16))

$$\begin{aligned}\frac{m_t^{\rm ren.}}{\Lambda} &= \frac{m_t^{\rm bare}}{\Lambda} + \left(\frac{a}{4N_{\rm c}}\right)\int_0^1 \frac{dw}{[1-a\mathcal{J}_H(w,x^2)]}\Big[\frac{1}{4x^3}w\left(w+2x^2-\sqrt{w(w+4x^2)}\right) + \\ &\quad + \frac{1}{x}\left(w-\sqrt{w(w+4x^2)}\right)\Big] + \frac{(\delta m_t)^{\rm QCD}}{\Lambda} \ , \end{aligned} \qquad (39)$$

where we employed the notation

$$x = \frac{m_t}{\Lambda} = \frac{m_t^{\rm bare}}{\Lambda} \ ,$$

and w is the square of the 4-momentum $\bar{p}/\Lambda$ of the (non-dynamical) Higgs H appearing in Figs. 5a-c (cf. (C.14)). The $(\delta m_t)^{\rm QCD}$ can be obtained from (C.16). For the case of the simple Pauli-Villars subtraction this yields

$$(\delta m_t)^{\rm QCD}_{\rm P.V.} = \frac{\alpha_{\rm s}}{\pi} m_t \ln\left(\frac{\Lambda^2}{m_t^2}\right) \ , \qquad (40)$$

and for the case of the "proper time" cut-off this gives

$$(\delta m_t)^{\rm QCD}_{\rm p.t.} = \frac{\alpha_{\rm s}}{\pi} m_t \left[\ln\left(\frac{\Lambda^2}{m_t^2}\right) + 0.2561... + \frac{5}{9}\frac{m_t^2}{\Lambda^2} + \mathcal{O}\left(\frac{m_t^4}{\Lambda^4}\right)\right] \ . \qquad (41)$$

The logarithmic terms in (40) and (41) can be reproduced by using the 1-loop renormalization group equation of the Standard Model for the top quark Yukawa coupling, by ignoring all the terms contributing to the running of that coupling except those of QCD.

The renormalized quantities $(m_t^{\rm ren.}/\Lambda)$, which correspond to the full bare values (m_t/Λ) of the third column of Table 1, were calculated from (39) numerically, using for $(\delta m_t)^{\rm QCD}$ again the "proper time" cut-off (41). They are given in the adjacent fourth column of Table 1. For the case without the QCD contributions (the fifth column), the corresponding renormalized quantities are in the adjacent sixth column - calculated from (39) without the $(\delta m_t)^{\rm QCD}$ term. The $(0+1)$-loop bare mass $m_t^{(1)}$ (second column) does not get renormalized at this level, since we remain in this case only at the leading order level in the $1/N_{\rm c}$-expansion.

The result (35) and Table 1 imply, within our framework, that the symmetry breaking (condensation) occurs only for

$$\frac{m_t^{\text{ren.}}}{\Lambda} \gtrsim 0.217\ (0.213) \qquad \Rightarrow \qquad \Lambda \lesssim 4.6 m_t^{\text{ren.}}\ (4.7 m_t^{\text{ren.}})\ . \tag{42}$$

The values in brackets correspond to the case when no QCD effects are included. For $m_t^{\text{ren.}}$ with the value of $180 \mathrm{G}eV$ [13], we obtain within the present framework the main result of our paper: there is an upper bound for the energy cut-off $\Lambda = E_{\text{condensation}}$

$$\Lambda \lesssim 0.830 \text{ TeV } (0.845 \text{ TeV})\ . \tag{43}$$

The value in the brackets corresponds to the case when the QCD effects are ignored. We see that the inclusion of the leading part of the QCD effects does not affect appreciably this upper bound. Furthermore, if we use in the QCD contributions instead of the "proper time" cut-off the simple Pauli-Villars subtraction, the results ($a_{\text{crit.}} \approx 1.48$, $m_t^{\text{ren.}}/\Lambda \gtrsim 0.215$) differ very little from the "proper time case" for the gluonic contributions ($a_{\text{crit.}} \approx 1.50$, $m_t^{\text{ren.}}/\Lambda \gtrsim 0.217$).

If we take instead of the requirement of the disappearance of the minimum (cf. (35)) a more conservative point of view, namely, the requirement that the calculated corrections to the 1-loop gap equation solution z_1 should not drastically change it (not by more than factor 2, cf. (37)), then the resulting upper bound on Λ is quite close to the above result

$$z > \frac{z_1}{2} \Rightarrow \frac{m_t^{\text{ren.}}}{\Lambda} \gtrsim 0.241\ (0.237) \Rightarrow \Lambda \lesssim 0.75 \text{ TeV } (0.76 \text{ TeV})\ . \tag{44}$$

Other authors [14] have studied next-to-leading order corrections in the $1/N_{\text{c}}$-expansion to the gap equation in four dimensions. They have considered only the two-loop contributions, which by themselves do not represent all the next-to-leading order contributions. They did not obtain an upper bound for Λ. The authors of [14] dealt mainly with the question of renormalizability of the model, i.e., of the viability of the limit $\Lambda \to \infty$. The related question of whether the quadratic divergences cancel exactly in the TSM has recently been investigated [15], with a goal of selecting $\Lambda \gg \mathcal{O}(\text{TeV})$.

Dealing with the cut-off Λ as a physical finite quantity was crucial in the present paper. We used for the integrals in the non-QCD sector (e.g. in calculating $\mathcal{J}_H(\bar{p}^2, \varepsilon^2)$) the simple spherical cut-off, corresponding to the following regions of integration for the diagrams of Fig. 3 and Figs. 5: $|\bar{p}|, |\bar{k}^{(1)}|, \ldots, |\bar{k}^{(\ell)}| \leq \Lambda$. It is a general fact that changing the cut-off prescription (e.g. using Pauli-Villars cut-offs in $\mathcal{J}_H$), or imposing the simple cut-off on some other combinations of the momenta (e.g. $|\bar{p} + \bar{k}^{(j)}| \leq \Lambda$, instead of $|\bar{k}^{(j)}| \leq \Lambda$), would modify numerical results [16]. This would affect quantitatively also the numerical results presented here. However, the main qualitative features (e.g. $\Lambda = \mathcal{O}(\text{TeV})$) seem to remain independent of the details of the cut-off prescription. This is suggested also by the fact that the calculated QCD contributions (which are numerically less important than those of the non-QCD, i.e., the scalar contributions) are only mildly dependent of whether we use for $\mathcal{J}_{\text{gl}}(\bar{p}^2, \varepsilon^2)$ the "proper time" cut-off (30) or the simple Pauli-Villars subtraction (29).

The effects of the loops of massive electroweak gauge bosons (i.e., their transverse and longitudinal degrees of freedom), the scalar contributions of even higher order in $1/N_{\text{c}}$ ($N_{\text{c}} = 3$) , as well as dynamical effects of the new physics beyond this relatively low Λ, have not been investigated here. The present results imply that QCD is playing a subordinate role in the condensation mechanism, and suggest that in the Top-mode Standard Model (TSM) there are the following two possibilities:

- The $1/N_{\text{c}}$-expansion of the contributions from the scalar sector [7] to V_{eff} yields a convergent or at least an asymptotic series, for $N_{\text{c}} = 3$. In this case, the next-to-leading order does not drastically change the gap equation. Consequently, as shown in the present paper, in such a case the decomposition of the $\langle \bar{t}t \rangle$ condensate into the constituent quarks should occur at a relatively *low* energy $\Lambda = \mathcal{O}(1\text{TeV})$.

- The second possibility occurs when $\Lambda > \mathcal{O}(1 \text{ TeV})$. Then $1/N_{\text{c}}$-expansion (for $N_{\text{c}} = 3$) mentioned above is neither convergent nor asymptotic, and already the next-to-leading order drastically changes the gap equation. Consequently, the leading order approximation loses its significance. We then appear to be in a strongly interacting region – the $\langle \bar{t}t \rangle$ condensates appear to interact strongly. The traditional methods of investigation (e.g. the method of calculating V_{eff}, tadpole approach, etc.) are insufficient in this case.

Acknowledgment

This work was supported in part by the Deutsche Forschungsgemeinschaft and in part by the European Union Science Project SC1-CT91-0729. E.A.P. wishes to thank W.A. Bardeen, N.D.V. to E.G. Floratos, and G.C. to Y.-L. Wu for illuminating discussions.

---

[7] Here we keep QCD contributions aside; they are smaller and can apparently be organized into a convergent or at least asymptotic loop series in powers of $\alpha_s(m_t)$; cf. last paragraph of Section 3.

Appendix A Tracing in the momentum space

In the 4-dimensional Euclidean space we have the following coordinates and momenta: $\bar{x} = (ix^0, x^j)$; $\bar{q} = (-iq^0, -q^j)$. We denote by $|\bar{x}\rangle$ and $|\bar{q}\rangle$ the normalized coordinate and momentum eigenstates. Then the following relations hold:

$$\langle \bar{x'}|\bar{x}\rangle = \delta^{(4)}(\bar{x} - \bar{x'}) \ , \quad \langle \bar{q'}|\bar{q}\rangle = \delta^{(4)}(\bar{q} - \bar{q'}) \ , \quad \langle \bar{x}|\bar{q}\rangle = (2\pi)^{-2} e^{-i\bar{x}\cdot\bar{q}} \ .$$

$$\int d^4\bar{x} |\bar{x}\rangle\langle\bar{x}| = \int d^4\bar{q} |\bar{q}\rangle\langle\bar{q}| = 1 \ . \tag{A.1}$$

The trace of an operator $\hat{C}$ can then easily be rewritten in the momentum space

$$Tr\hat{C} \left(= \int d^4\bar{x} \langle\bar{x}|\hat{C}|\bar{x}\rangle \right) = \int d^4\bar{q} \langle\bar{q}|\hat{C}|\bar{q}\rangle \ . \tag{A.2}$$

For many operators it is easier to work in the momentum space than in the $\bar{x}$-space - e.g. the operator $\ln \hat{\mathcal{A}}$, if $\hat{\mathcal{A}}$ is translationally invariant and non-diagonal in the $\bar{x}$-space. Then the operator $\ln \hat{\mathcal{A}}$ is diagonal in the momentum space and easier to work with in this space. When calculating the trace of such operators, we use (A.2) in the momentum basis. All those operators $\hat{C}$ which are translationally invariant in the $\bar{x}$-space are diagonal in the momentum space

$$\langle \bar{x'}|\hat{C}|\bar{x}\rangle = \langle \bar{0}|\hat{C}|\bar{x} - \bar{x'}\rangle \quad \Rightarrow \quad \langle \bar{q'}|\hat{C}|\bar{q}\rangle = \delta^{(4)}(\bar{q} - \bar{q'})\tilde{C}(\bar{q}) \ , \ \text{where: } \tilde{C}(\bar{q}) = \int d^4\bar{x} e^{-i\bar{q}\cdot\bar{x}} \langle\bar{0}|\hat{C}|\bar{x}\rangle \ . \tag{A.3}$$

The trace of such an operator can be obtained from (A.2), once we know the Fourier-transform $\tilde{C}(\bar{q})$

$$Tr\hat{C} = (2\pi)^{-4}\Omega \int d^4\bar{q}\tilde{C}(\bar{q}) \ , \quad \text{where: } \ \Omega = (2\pi)^4 \lim_{\bar{q}\to 0} \delta^{(4)}(\bar{q}) = \int d^4\bar{x} \ . \tag{A.4}$$

It is straightforward to check that for any power of such an operator $\hat{C}$ we have

$$\langle \bar{q'}|\hat{C}^n|\bar{q}\rangle = \delta^{(4)}(\bar{q} - \bar{q'})(\tilde{C}(\bar{q}))^n \qquad (n = 0, \pm 1, \pm 2, \ldots) \ . \tag{A.5}$$

The operator $\hat{B}[\sigma_0]$, as defined by (9) and (10), is translationally invariant. Therefore

$$\langle \bar{q'}; j, a|\hat{B}[\sigma_0]|\bar{q}; k, b\rangle = \delta^{(4)}(\bar{q} - \bar{q'})\tilde{B}_0(\bar{q}; j, k; a, b) \ ,$$

$$\tilde{B}_0(\bar{q}; j, k; a, b) = \delta_{ab}\delta_{jk}(-\bar{\not{q}} + \delta_{j1}\lambda\sigma_0) \ , \quad \text{where: } \bar{\not{q}} = \bar{\gamma}^\mu \bar{q}^\mu \ (\bar{\gamma}^0 = i\gamma^0, \ \bar{\gamma}^j = \gamma^j). \tag{A.6}$$

In order to calculate $Tr(\ln \hat{B}[\sigma_0])$ of eq. (13), we note first that $\ln \hat{B}[\sigma_0]$ can be written as a Taylor series in powers of $(\hat{B}[\sigma_0] - 1)$. Applying to these powers relation (A.5), we obtain

$$\langle \bar{q'}; j, a| \ln \hat{B}[\sigma_0]|\bar{q}; k, b\rangle = \delta^{(4)}(\bar{q} - \bar{q'})\delta_{ab}\delta_{jk} \ln(-\bar{\not{q}} + \delta_{j1}\lambda\sigma_0) \ . \tag{A.7}$$

Applying now the relations (A.2) and (A.4), we obtain $Tr(\ln \hat{B}[\sigma_0])$

$$Tr \ln \hat{B}[\sigma_0] == (2\pi)^{-4} \Omega N_{\rm c} tr_{\rm f} \int d^4\bar{q} \ln \left(-\not{\bar{q}} + \lambda\sigma_0\right) + \cdots \ , \tag{A.8}$$

where the dots represent an σ_0-independent term (corresponding to the isospin index $j = 2$), which is irrelevant for $V_{\rm eff}^{(1)}(\sigma_0)$. The factor $N_{\rm c}$ (the number of colors) comes from summing over the color indices a, b. (A.8) gives us the result on the r.h.s. of eq. (13) (replace: $\bar{q} \mapsto -\bar{k}$).

Next we derive the result of eq. (20). The operator $\hat{A}$, which was introduced in eq. (15), was defined through the relation (16), or equivalently (see eqs. (12) and (15))

$$2 \int d^4\bar{x} \sigma_1(\bar{x})^2 + \lambda^2 Tr[(\hat{B}[\sigma_0]^{-1}\hat{\sigma}_1)^2] = \int d^4\bar{x} d^4\bar{x}' \sigma_1(\bar{x}') \langle \bar{x}' | \hat{A} | \bar{x} \rangle \sigma_1(\bar{x}) \ . \tag{A.9}$$

In order to obtain the expression for the matrix element $\langle \bar{x}' | \hat{A} | \bar{x} \rangle$, we must calculate $Tr[(\hat{B}[\sigma_0]^{-1}\hat{\sigma}_1)^2]$. First, we use (A.2) and repeatedly apply the completeness insertions (A.1)

$$\begin{aligned} Tr[(\hat{B}[\sigma_0]^{-1}\hat{\sigma}_1)^2] = \langle \bar{q} | \hat{B}[\sigma_0]^{-1} | \bar{q}^{(1)} \rangle \langle \bar{q}^{(1)} | \bar{x}^{(1)} \rangle \langle \bar{x}^{(1)} | \hat{\sigma}_1 | \bar{x}^{(2)} \rangle \langle \bar{x}^{(2)} | \bar{q}^{(2)} \rangle \times \\ \times \langle \bar{q}^{(2)} | \hat{B}[\sigma_0]^{-1} | \bar{q}^{(3)} \rangle \langle \bar{q}^{(3)} | \bar{x}^{(3)} \rangle \langle \bar{x}^{(3)} | \hat{\sigma}_1 | \bar{x}^{(4)} \rangle \langle \bar{x}^{(4)} | \bar{q} \rangle \ . \end{aligned} \tag{A.10}$$

Here, we implicitly assume integrations over all momenta ($\bar{q}$, $\bar{q}^{(1)}$, $\ldots$) and coordinates ($\bar{x}^{(1)}$, $\bar{x}^{(2)}$, $\ldots$). Furthermore, the color, isospin and spinor degrees of freedom were omitted in the notation of (A.10); summation over these indices and tracing over spinor degrees of freedom ($tr_{\rm f}$) is implicitly assumed. The matrix elements of $\hat{B}[\sigma_0]^{-1}$, which appear on the r.h.s. of (A.10), are obtained from (A.6) and (A.5) (for $n = -1$). Using in addition (A.1) for $\langle \bar{x} | \bar{q} \rangle$, and the locality of the quantum fluctuation operator $\hat{\sigma}_1$ (i.e., $\langle \bar{x}' | \hat{\sigma}_1 | \bar{x} \rangle = \sigma_1(\bar{x}) \delta^{(4)}(\bar{x} - \bar{x}')$), we obtain from (A.10) after some bookkeeping

$$Tr[(\hat{B}[\sigma_0]^{-1}\hat{\sigma}_1)^2] = N_{\rm c} tr_{\rm f} \int d^4\bar{x} d^4\bar{x}' \sigma_1(\bar{x}') \sigma_1(\bar{x}) \int \frac{d^4\bar{q} d^4\bar{q}'}{(2\pi)^8} \frac{\exp\left[i\left(\bar{q} - \bar{q}'\right) \cdot \left(\bar{x} - \bar{x}'\right)\right]}{(-\not{\bar{q}} + \lambda\sigma_0)(-\not{\bar{q}}' + \lambda\sigma_0)} + \cdots \ . \tag{A.11}$$

Here, the factor $N_{\rm c}$ came from tracing over the color degrees of freedom. Dots represent a term independent of σ_0 (corresponding to the isospin indices $j = k = 2$), i.e., this term is irrelevant for $V_{\rm eff}(\sigma_0)$ (cf. eq. (12)). Performing in (A.11) the replacements $\bar{q}' \to \bar{k}$, $\bar{q} \to \bar{p} + \bar{k}$, combining the obtained expression with the relation (A.9), and introducing a physical energy cut-off $(\bar{k}^2)_{max} = \Lambda^2$, we immediately obtain the result of eq. (20), i.e., the explicit expression for the matrix element $\langle \bar{x}' | \hat{A} | \bar{x} \rangle$, its Fourier transform $\tilde{A}(\bar{p})$ and the related function $\mathcal{K}_H(\bar{p}^2, \lambda^2\sigma_0^2)$. Note that the operator $\hat{A}$ is the kernel for the quadratic quantum fluctuations of the Higgs field around the minimum.

Finally, according to eq. (19), $Tr \ln \hat{A}$ remains to be calculated in order to obtain $V_{\rm eff}^{(\rm ntl)}$. This can be done now, by using the same approach as in (A.8) for calculating $Tr \ln \hat{B}[\sigma_0]$

$$Tr \ln \hat{A} = (2\pi)^{-4} \Omega \int d^4\bar{p} \ln \tilde{A}(\bar{p}) = (2\pi)^{-4} \Omega \int d^4\bar{p} \ln[1 - 2\lambda^2 N_{\rm c} \mathcal{K}_H(\bar{p}^2, \lambda^2\sigma_0^2)] + \cdots \ , \tag{A.12}$$

where the dots represent an irrelevant σ_0-independent term. This time the trace is performed only over the 4-momentum space, because the operator $\hat{A}$ (eq. (20)) has no color, isospin or spinor degrees of freedom any more. Using the relation $d^4\bar{p} = \pi^2 d\bar{p}^2 \bar{p}^2$ (the integrand in (A.12) is spherically symmetric), introducing a physical energy cut-off $(\bar{p}^2)_{max} = \Lambda^2$, and rescaling the momentum $\bar{p}^2 \mapsto \Lambda^2 \bar{p}^2$, leads directly to the final result (21) and (22). This is the next-to-leading order (beyond 1-loop) contribution of the composite Higgs sector to the effective potential.

Appendix B J functions for the effective potential

The function $\mathcal{J}_H(\bar{p}^2, \varepsilon^2)$, which is needed for calculating the $V_{\rm eff}^{\rm (ntl)}$ in eq. (21) and is given in an integral form in eq. (22), can be calculated analytically. In the 4-dimensional Euclidean space, we can write

$$\bar{p} \cdot \bar{k} = |\bar{p}||\bar{k}| \cos\theta \ , \quad d^4\bar{k} = (2\pi)|\bar{k}|^2 \sin^2\theta d|\bar{k}|^2 d\theta \qquad (0 \leq \theta \leq \pi) \ . \tag{B.1}$$

The integration over θ in (22) can be performed by using (cf. Ryzhik and Gradshteyn, 3.644/4)

$$\int_0^\pi \frac{d\theta \sin^2\theta}{(\mathcal{A} + \mathcal{B}\cos\theta)} = \pi \frac{\mathcal{A}}{\mathcal{B}^2} \left[1 - \sqrt{(1 - \frac{\mathcal{B}^2}{\mathcal{A}^2})} \right] \ . \tag{B.2}$$

Subsequently, the radial integration over $|\bar{k}|^2$ in (22) is performed by using well-known formulas (e.g. Ryzhik and Gradshteyn, 2.261, 2.266, 2.267). It leads to the result

$$\begin{aligned} \mathcal{J}_H(\bar{p}^2, \varepsilon^2) = \Big\{ & \frac{3}{4} - \frac{1}{2}\varepsilon^2 \ln(\varepsilon^{-2} + 1) + \frac{(1+\varepsilon^2)^2}{8\bar{p}^2} - \frac{\bar{p}^2}{8} - \frac{(1 - \bar{p}^2 + \varepsilon^2)}{8\bar{p}^2}\mathcal{B} - \frac{\varepsilon^2}{2} \ln\left(\frac{a_3}{2\varepsilon^2}\right) \\ & - \frac{1}{4}(\bar{p}^2 + 4\varepsilon^2) \left[1 + \frac{(1 + \varepsilon^2 - \mathcal{B})}{\bar{p}^2} + (1 - \mathcal{A}) \ln(\varepsilon^{-2} + 1) + \mathcal{A} \ln\left(\frac{a_1}{a_2}\right) + \ln\left(\frac{a_3}{2\varepsilon^2}\right) \right] \Big\} \ , \end{aligned} \tag{B.3}$$

$$\text{where:} \qquad \mathcal{A} = \sqrt{1 + 4\frac{\varepsilon^2}{\bar{p}^2}} \ , \qquad \mathcal{B} = \sqrt{(1 - \bar{p}^2 + \varepsilon^2)^2 + 4\bar{p}^2\varepsilon^2} \ ,$$

$$a_1 = (\bar{p}^2 + 3\varepsilon^2 - 1 + \mathcal{A}\mathcal{B}) \ , \quad a_2 = \bar{p}^2 + 3\varepsilon^2 + (\bar{p}^2 + \varepsilon^2)\mathcal{A} \ , \quad a_3 = 1 - \bar{p}^2 + \varepsilon^2 + \mathcal{B} \ . \tag{B.4}$$

The partial derivative $\partial\mathcal{J}_H/\partial\varepsilon^2$, which appears in an integrand of the gap equation (34), is

$$\begin{aligned} \frac{\partial\mathcal{J}_H(\bar{p}^2, \varepsilon^2)}{\partial\varepsilon^2} = \Big\{ & \frac{(\bar{p}^2 + 6\varepsilon^2)}{4\varepsilon^2(1 + \varepsilon^2)} - \frac{(\bar{p}^2 + \varepsilon^2)(\bar{p}^2 + 7\varepsilon^2)}{4\bar{p}^2\varepsilon^2} - \frac{3}{4\bar{p}^2} + \frac{\mathcal{B}(3 + \bar{p}^2 + 7\varepsilon^2)}{4\bar{p}^2(1 + \varepsilon^2)} \\ & - \frac{3}{2}\ln\left(\frac{a_3}{2}\right) - \frac{3}{2}\mathcal{A}\ln\left(\frac{a_1}{a_2}\right) + \frac{3}{2}(\mathcal{A} - 1)\ln(1 + \varepsilon^2) + \frac{3}{2}(2 - \mathcal{A})\ln\varepsilon^2 \Big\} \ , \end{aligned} \tag{B.5}$$

where the notations of (B.4) are used. This expression can be obtained by the same method as (B.3), or by direct differentiation of (B.3). A form of $\mathcal{J}_H(\bar{p}^2, \varepsilon^2)$ accurate up to $\mathcal{O}(\varepsilon^4 \ln \varepsilon^2)$ (note:

$\bar{p}^2,\ \varepsilon^2\ \propto\ 1/\Lambda^2$) is

$$\mathcal{J}_H(\bar{p}^2,\varepsilon^2) = \Big\{ \left(1 - 2\varepsilon^2 + 3\varepsilon^2 \ln \varepsilon^2\right) + \bar{p}^2 \left(-\frac{3}{4} + \frac{1}{2}\ln\varepsilon^2 - \frac{1}{2}\varepsilon^2\right) - \\ -\frac{1}{2}\bar{p}^2 \left(1 + \frac{4\varepsilon^2}{\bar{p}^2}\right)^{3/2} \ln\left[1 + \frac{\bar{p}^2}{2\varepsilon^2} - \sqrt{\frac{\bar{p}^2}{\varepsilon^2}\left(1 + \frac{\bar{p}^2}{4\varepsilon^2}\right)}\right] + \mathcal{O}\left(\varepsilon^4 \ln\varepsilon^2\right) \Big\} \ . \tag{B.6}$$

Furthermore, the $\mathcal{J}_H(\bar{p}^2 = 0, \varepsilon^2)$ can be obtained either from (B.3), or by direct spherical integration

$$\mathcal{J}_H(\bar{p}^2 = 0, \varepsilon^2) = \left[1 - 3\varepsilon^2 \ln(\varepsilon^{-2} + 1) + \frac{2\varepsilon^2}{1+\varepsilon^2}\right] \ . \tag{B.7}$$

The expression for α (eq. (18)) was assumed to be positive, because otherwise the path integral derivation of $V_{\text{eff}}^{(\text{ntl})}$ presented there would not be mathematically justifiable

$$\alpha = \frac{\Omega}{\tilde{A}(\bar{p} = 0, \lambda^2\sigma_0^2)}\ >\ 0 \quad \Rightarrow \quad aJ(\bar{p}^2 = 0, \varepsilon^2)\ <\ 1 \quad \left(a = \frac{G N_{\text{c}} \Lambda^2}{8\pi^2} \sim 1\right) . \tag{B.8}$$

It can be checked numerically that for $(0 \leq \bar{p}^2, \varepsilon^2 \leq 1)$ the function $\mathcal{J}_H(\bar{p}^2,\varepsilon^2)$ has the following properties: $\mathcal{J}_H(\bar{p}^2,\varepsilon^2) \leq 1$, where the equality holds only at $\bar{p}^2 = \varepsilon^2 = 0$; $\mathcal{J}_H(\bar{p}^2,\varepsilon^2)$ is a monotonously decreasing function of $\bar{p}^2$ if $\varepsilon^2 < 0.63$. Hence, (B.8) implies the general condition

$$a\mathcal{J}_H(\bar{p}^2,\varepsilon^2)\ <\ 1 \qquad \text{for all:}\ \ (0 \leq \bar{p}^2 \leq 1)\ . \tag{B.9}$$

However, this is precisely the condition that the expression $V_{\text{eff}}^{(\text{ntl})}$ in eq. (21) does not contain any singularities in the integrand. Therefore, the condition $\alpha > 0$, which was needed so that the derivation of $V_{\text{eff}}^{(\text{ntl})}$ by path integral method was mathematically consistent, guarantees also that the obtained result is mathematically well-behaved. From the diagrammatic point of view (Appendix C), the condition (B.9) means that the diagrammatic sum of the next-to-leading order terms in the $1/N_{\text{c}}$-expansion contributing to the effective potential (i.e., $V_{\text{eff}}^{(\text{ntl})}$) does not diverge (cf. eqs. (C.9), (C.10)), and in fact leads to the logarithm in the integrand of eq. (21). The "non-singularity" condition (B.9) holds safely for all such ε^2 which satisfy

$$\varepsilon^2\ >\ 0.25 z_1 \qquad \left(z_1 = \left(m_t^{(1)}/\Lambda\right)^2\right)\ , \tag{B.10}$$

where z_1 is the solution of the $(0+1)$-loop gap equation. The mentioned singularities appear in Figs. 1a-1e as poles of $V_{\text{eff}}(\varepsilon^2)$ (full lines) in these regions of small ε^2 – features which are not physical, but represent some artifacts of the mathematical approach of the present paper – namely, the $1/N_{\text{c}}$-expansion in the electroweak sector. In any way, if the calculated $1/N_{\text{c}}$-corrections to V_{eff} were to change the position of the minimum z as drastically as by factor 4 or more, i.e., if singularities were to appear near the new minimum (cf. (B.10)), then the expansion of the electroweak contributions to $V_{\rm eff}$ in powers of $1/N_{\rm c}$ would be a highly divergent and senseless series, anyway. Since these singularities always lie safely away from the minima of the effective potential ($\varepsilon^2 \approx z$) given in Table 1, they do not influence the conclusions about the value and the existence of this minimum in any appreciable way, and are hence irrelevant for the purpose of the present paper. In Figs. 1a-1e we have not continued the (full) lines of $V_{\rm eff}$ into these singular small-ε^2 regions.

The integrals (28)-(30), connected with the dominant gluonic contribution to $V_{\rm eff}$, have also explicit solutions. The resulting function $\mathcal{J}_{\rm gl}$ (cf. (27)-(32)) is in the case of one simple Pauli-Villars cut-off

$$\begin{aligned}
\mathcal{J}_{\rm gl}^{(\rm P.V.)}\left(\bar{p}^2,\varepsilon^2\right) &= \int_0^1 dz z(1-z)\ln\left[\frac{z(1-z)\bar{p}^2+\varepsilon^2}{z(1-z)\bar{p}^2+1}\right] \\
&= -\frac{1}{6}\left(2\frac{\varepsilon^2}{\bar{p}^2}-1\right)\mathcal{D}\left(\frac{\varepsilon^2}{\bar{p}^2}\right)+\frac{1}{6}\ln\varepsilon^2+\frac{1}{6}\left(2\frac{1}{\bar{p}^2}-1\right)\mathcal{D}\left(\frac{1}{\bar{p}^2}\right) \ , \qquad \text{(B.11)}
\end{aligned}$$

and in the case of the “proper time” cut-off

$$\begin{aligned}
\mathcal{J}_{\rm gl}^{(\rm p.t.)}\left(\bar{p}^2,\varepsilon^2\right) &= -\frac{1}{6}\left(2\frac{\varepsilon^2}{\bar{p}^2}-1\right)\mathcal{D}\left(\frac{\varepsilon^2}{\bar{p}^2}\right)+\frac{1}{6}\ln\varepsilon^2+\frac{2}{9} \\
&\quad -\frac{1}{6}\left(\frac{\bar{p}^2}{5}+\varepsilon^2\right)+\frac{1}{4}\left(\frac{\bar{p}^4}{140}+\frac{\bar{p}^2\varepsilon^2}{15}+\frac{\varepsilon^4}{6}\right)+\mathcal{O}\left(\bar{p}^6,\varepsilon^6\right) \ . \qquad \text{(B.12)}
\end{aligned}$$

Here we denoted by $\mathcal{D}$ the integral

$$\mathcal{D}\left(w\right)=\int_0^1 dz\ln\left[1+\frac{z(1-z)}{w}\right]=-2+\sqrt{(4w+1)}\ln\left[\frac{\sqrt{(4w+1)}+1}{\sqrt{(4w+1)}-1}\right] \ . \qquad \text{(B.13)}$$

The corresponding derivatives $\partial\mathcal{J}_{\rm gl}(\bar{p}^2,\varepsilon^2)/\partial\varepsilon^2$ are obtained in a straightforward manner from the above expressions, by using also the following integral

$$\frac{d\mathcal{D}\left(w\right)}{dw}=-\frac{1}{w}+\frac{2}{\sqrt{(4w+1)}}\ln\left[\frac{\sqrt{(4w+1)}+1}{\sqrt{(4w+1)}-1}\right] \ . \qquad \text{(B.14)}$$

We note that, unlike $\mathcal{J}_H$, the gluonic function $\mathcal{J}_{\rm gl}$ is negative in the entire region of $\bar{p}^2$ and ε^2 of our interest, and therefore does not lead to any possible singularities in the logarithm of $V_{\rm eff}^{(\rm gl)}$ in (31).

Appendix C Diagrammatic derivation of $V_{\rm eff}^{(\rm ntl)}$; mass renormalization

In this Appendix we show that $V_{\rm eff}^{(\rm ntl)}$ of eq. (21) can be rederived by a diagrammatic method and, in addition, that it represents precisely all the effects of loops which are next-to-leading order in the formal $1/N_\mathrm{c}$-expansion (these are terms beyond one loop). It is evident from eq. (24) that the 4-fermion coupling G is of order $1/N_\mathrm{c}$ (for a fixed Λ^2). This fact will be used repeatedly throughout this Appendix.

We will use the original notations of the Lagrangian (2), in order to see explicitly that the dependence of the results on the undetermined bare mass M_0 drops out. Furthermore, we will introduce $g = M_0\sqrt{G}$ which is dimensionless. We employ the usual diagrammatic method for V_eff [11], which has been applied in ref. [10] to the 1-loop graphs.

$$V_\mathrm{eff}(H_0) = i \sum_{m=1}^{\infty} \frac{1}{(2m)!} \tilde{\Gamma}_H^{(2m)}(p_1, \ldots, p_{2m})\Big|_{(\{p_k\}=\{0\})} H_0^{(2m)} \ . \tag{C.1}$$

Here, $\tilde{\Gamma}_H^{(2m)}$'s are 1-PI Green functions corresponding to the diagrams of the Lagrangian (2) with $2m$ outer legs of the (yet non-dynamical) Higgs H_0 fields with zero momenta[8]. The 1-loop diagrams contributing to $\tilde{\Gamma}_H^{(2m)}$'s are depicted in Figs. 2a-2c, and they lead to $V_\mathrm{eff}^{(1)}$ of eq. (14) [10]. The $(\ell+1)$-loop 1-PI diagrams contributing to $\tilde{\Gamma}_H^{(2m)}$ are depicted in Fig. 3. We note that *no* other $(\ell+1)$-loop 1-PI diagrams are next-to-leading order in the formal $1/N_\mathrm{c}$-expansion. For example, the 3-loop and 4-loop 1-PI diagrams of Figs. 4a-4b (when the external legs are cut away) are not proportional to $(G^2N_\mathrm{c}^2)$, $(G^3N_\mathrm{c}^3)$ $(= \mathcal{O}(1))$, but rather to (G^2N_c), $(G^3N_\mathrm{c}^2)$ $(= \mathcal{O}(1/N_\mathrm{c}))$, respectively. On the other hand, the diagrams in Fig. 3 (when the external legs are cut out) are proportional to $\mathcal{O}(1)$, i.e., they are next-to-leading order in the $1/N_\mathrm{c}$-expansion. We can understand this by counting the number of quark loops and of Yukawa couplings. In Fig. 3, the total number of loops is $(\ell+1)$, and the number of (top) quark loops among them is $n_q = \ell$. In all other 1-PI diagrams with the total number of loops $(\ell+1)$ (e.g. those in Figs. 4a-4b) is the number of (top) quark loops less than ℓ: $n_q < \ell$. On the other hand, the number of Yukawa couplings is 2ℓ in all 1-PI diagrams with the total number of loops $(\ell+1)$, and therefore the Yukawa couplings yield a factor $(\sqrt{G})^{2\ell}$. Each quark loop gives a factor N_c by tracing over the color degrees of freedom. The $2m$ external Higgs lines give the factor $(gH_0)^{2m}$ $(g = \sqrt{G}M_0)$ [9]. In total, this gives contributions to V_eff of (C.1) proportional to $(G^\ell N_\mathrm{c}^{n_q})(gH_0)^{2m} = \mathcal{O}(1/N_\mathrm{c}^{\ell-n_q})(gH_0)^{2m}$. In the case of the diagrams of Fig. 3, $\mathcal{O}(1/N_\mathrm{c}^{\ell-n_q})$ is $\mathcal{O}(1)$, in the case of other diagrams (e.g. those of Figs. 4a-4b) we have $\mathcal{O}(1/N_\mathrm{c}^{\ell-n_\mathrm{f}}) \leq \mathcal{O}(1/N_\mathrm{c})$. Thus, all 1-PI diagrams with $(\ell+1)$ loops and $\ell \geq 1$, other than those of Fig. 3, give contributions to $V_\mathrm{eff}(gH_0)$ which are of lower order than the next-to-leading order terms in in the $1/N_\mathrm{c}$-expansion. Therefore, we will ignore all such diagrams. We note in passing that there is only one 1-PI diagram with two loops, and it is of the type depicted in Fig. 3, i.e., of the next-to-leading order in the $1/N_\mathrm{c}$-expansion.

---

[8] It will be shown later in this Appendix that diagrams with an odd number of H_0-outer legs do not contribute.

[9] The parameter $\varepsilon^2 = (gH_0)^2/(2\Lambda^2)$ (cf. eq. (22)) turns out to be the natural variable of $\mathcal{O}(1/N_\mathrm{c}^0)$ in V_eff.

The 1-PI Green function resulting from the $(\ell+1)$-loop diagrams with $(2m)$-outer Higgs legs of Fig. 3 can be written as

$$\tilde{\Gamma}_H^{(2m;\ell+1)}(p_1, \ldots, p_{2m})\Big|_{(\{p_j\}=\{0\})} = \sum_{\substack{m_1,\ldots,m_\ell \geq 0 \\ m_1+\cdots m_\ell = m}} \mathcal{G}_{m_1 \cdots m_\ell} \ . \tag{C.2}$$

Here, the $(2m)$ external Higgs lines are distributed among the quark loops as follows: each term $\mathcal{G}_{m_1 \cdots m_\ell}$ represents the contribution of those diagrams of Fig. 3 which have on their ℓ loops of massless (top) quarks $2m_1, \ldots, 2m_\ell$ outer H_0-legs with zero momenta, respectively. Hence:

$$\mathcal{G}_{\substack{m_1 \cdots m_\ell \\ (m_1+\cdots+m_\ell=m)}} = \frac{i^{2m+2\ell}}{(2m+2\ell)!} N_{\mathrm{c}}^{\ell} (-1)^{\ell} \left(-\frac{g}{\sqrt{2}}\right)^{2m+2\ell} \int \frac{d^4p d^4k^{(1)} \cdots d^4k^{(\ell)}}{(2\pi)^{4(\ell+1)}} \times$$
$$\left[\prod_{j=1}^{\ell} tr_{\mathrm{f}} \left(\sum_{n_j=0}^{2m_j} \frac{i^{2m_j+2}}{(\not{k}^{(j)})^{2m_j+1-n_j} (\not{p} + \not{k}^{(j)})^{n_j+1}} \right)\right] \times \left(\frac{i}{-M_0^2}\right)^{\ell} \times N_H^{\mathrm{in}} N_H^{\mathrm{out}} N_q \ . \tag{C.3}$$

Here, $k^{(j)}$ and $(p+k^{(j)})$ are the two momenta in the j^{th} (massless top) quark loop; p is the momentum of the ℓ internal Higgs propagators, and each such propagator is simply $(-i/M_0^2)$ (Higgses are non-dynamical); $(-g/\sqrt{2})$ is the Yukawa coupling (cf. eq. (2); $g = M_0\sqrt{G}$); $(-1)^\ell$ is the Fermi statistical factor from the ℓ quark-loops; N_{c}^{ℓ} is the factor arising from tracing over the colors of the ℓ quark loops; N_H^{in}, N_H^{out}, N_q are the numbers of possible contractions between the internal Higgs fields, between the external Higgs fields, and between the internal (top) quarks, respectively (in the framework of the formalism of the Wick theorem). We label each quark loop by the number j $(j = 1, \ldots, \ell)$. The j^{th} quark loop has altogether $2m_j$ external Higgs legs of momentum zero and two legs of internal Higgs propagators of momentum p attached to it. The external Higgs legs are distributed on this loop so that there are n_j legs attached to it outside the chain and $(2m_j - n_j)$ legs attached to it inside the chain (see Fig. 3). When performing the trace, we have to sum over all possible distributions of the external Higgs lines, i.e., varying n_j from 0 to $2m_j$. Incidentally, it follows from the above expression (C.3) that the numbers $2m_1, \ldots, 2m_\ell$ (and their sum $2m$, i.e., the number of external legs) must be even, because trace of a product of an odd number of γ matrices is zero.

Next, we must count carefully the contractions N_H^{in}, N_H^{out} and N_q, as dictated by the Wick theorem. We find

$$N_H^{\mathrm{in}} = \binom{2m+2\ell}{2}\binom{2m+2\ell-2}{2} \cdots \binom{2m+2}{2}\frac{1}{\ell!} = \frac{(2m+2\ell)!}{(2m)!(2!)^{\ell}\ell!} \ ,$$
$$N_H^{\mathrm{out}} = (2m)! \ , \qquad N_q = (2m)!(\ell-1)!2^{\ell-1} \ . \tag{C.4}$$

Using (C.1), (C.2) and (C.3), this gives us the following expression for those contributions of the $(\ell+1)$-loops $(\ell \geq 1)$ to the effective potential which are next-to-leading order in $1/N_{\mathrm{c}}$

$$V_{\mathrm{eff}}^{(\ell+1)-loops}(H_0) = \sum_{m=0}^{\infty} \left(\frac{GN_{\mathrm{c}}}{2}\right)^{\ell} \left(\frac{gH_0}{\sqrt{2}}\right)^{2m} \frac{i^{\ell+1}}{2\ell} \int \frac{d^4p d^4k^{(1)} \cdots d^4k^{(\ell)}}{(2\pi)^{4(\ell+1)}} \times$$

$$\sum_{\substack{m_1,\cdots,m_\ell \geq 0 \\ m_1+\cdots+m_\ell=m}} \left[\prod_{j=1}^{\ell} tr_{\mathrm{f}} \left(\sum_{n_j=0}^{2m_j} \frac{1}{(\not{k}^{(j)})^{2m_j+1-n_j}(\not{p}+\not{k}^{(j)})^{n_j+1}}\right)\right] . \qquad \text{(C.5)}$$

It is straightforward to see that for the expansion in powers of $(gH_0/\sqrt{2})$ the following crucial identity holds:

$$\prod_{j=1}^{\ell} tr_{\mathrm{f}} \left[\frac{1}{(\not{k}^{(j)} - \frac{gH_0}{\sqrt{2}})} \frac{1}{(\not{p}+\not{k}^{(j)} - \frac{gH_0}{\sqrt{2}})}\right] = \sum_{m=0}^{\infty} \left(\frac{gH_0}{\sqrt{2}}\right)^{2m} \times$$

$$\sum_{\substack{m_1,\cdots,m_\ell \geq 0 \\ m_1+\cdots+m_\ell=m}} \left[\prod_{j=1}^{\ell} tr_{\mathrm{f}} \left(\sum_{n_j=0}^{2m_j} \frac{1}{(\not{k}^{(j)})^{2m_j+1-n_j}(\not{p}+\not{k}^{(j)})^{n_j+1}}\right)\right] . \qquad \text{(C.6)}$$

This identity can be checked in a straightforward way by expanding the corresponding fractions on the l.h.s. in powers of $gH_0/(\sqrt{2}\not{k}^{(j)})$ and $gH_0/(\sqrt{2}(\not{p}+\not{k}^{(j)}))$. Here we note that this identity holds only as long as these two quantities have norms smaller than one. For small internal momenta k and/or $(p+k)$ (smaller than $(gH_0/\sqrt{2})$) [10], i.e., in the region of non-perturbative internal momenta, the above identity is, strictly speaking, not valid, because the perturbative "massless" sum on the r.h.s. is formally divergent in such a case. However, the "massive" l.h.s. is finite even for such small momenta, and it represents in this case the analytic continuation of the r.h.s. This identity, applied to (C.5), represents the window through which we get from a perturbative (diagrammatic) approach into the nonperturbative physics of the dynamical symmetry breaking - through analytic continuation.

Therefore, we can rewrite (C.5)

$$V_{\mathrm{eff}}^{(\ell+1)-loops}(H_0) = \frac{i}{2\ell} \int \frac{d^4p}{(2\pi)^4} \left[\int \frac{d^4k}{(2\pi)^4} \frac{iGN_{\mathrm{c}}}{2} tr_{\mathrm{f}} \left(\frac{1}{(\not{k} - \frac{gH_0}{\sqrt{2}})(\not{p}+\not{k} - \frac{gH_0}{\sqrt{2}})}\right)\right]^{\ell} . \qquad \text{(C.7)}$$

Performing Wick's rotation into the Euclidean metric ($d^4k \mapsto i d^4\bar{k}$, $\not{k} \mapsto \bar{\not{k}}$), we can rewrite the above integral over k in the Euclidean and cut-off regularized form

$$\int \frac{i d^4k}{(2\pi)^4} tr_{\mathrm{f}} \left(\frac{1}{(\not{k} - \frac{gH_0}{\sqrt{2}})(\not{p}+\not{k} - \frac{gH_0}{\sqrt{2}})}\right) =$$

---

[10] In the physically interesting region, i.e., near the minimum of V_{eff}, we have: $(gH_0/\sqrt{2}) \approx m_t$.

$$= - \int_{\bar{k}^2 \leq \Lambda^2} \frac{d^4 \bar{k}}{(2\pi)^4} tr_{\mathrm{f}} \left[\frac{1}{(\bar{\not{k}} - \frac{g H_0}{\sqrt{2}})(\bar{\not{p}} + \bar{\not{k}} - \frac{g H_0}{\sqrt{2}})} \right] = 4 \mathcal{K}_H(\bar{p}^2, H_0^2) \ . \tag{C.8}$$

Here we used the notation of eq. (20) for $\mathcal{K}_H$. Using further $d^4 p \mapsto i d^4 \bar{p}$ and rescaling $\bar{p}^2 (\leq \Lambda^2) \mapsto \Lambda^2 \bar{p}^2$ yields the integral

$$V_{\mathrm{eff}}^{(\ell+1)-loops}(H_0) = - \Lambda^4 \int_{\bar{p}^2 \leq 1} \frac{d^4 \bar{p}}{(2\pi)^4} \frac{1}{2\ell} \left[\frac{G N_{\mathrm{c}} \Lambda^2}{8\pi^2} \mathcal{J}_H(\bar{p}^2, \varepsilon^2) \right]^{\ell} \ , \tag{C.9}$$

where we employed the notation of eq. (22) for $\mathcal{J}_H$ and ε. Summing finally over $\ell = 1, 2, \ldots$ yields the logarithmic series and the result identical to $V_{\mathrm{eff}}^{(\mathrm{ntl})}$ of eq. (21)

$$\sum_{\ell=1}^{\infty} V_{\mathrm{eff}}^{(\ell+1)-loops}(H_0) = \frac{\Lambda^4}{2(4\pi)^2} \int_{\bar{p}^2 \leq 1} d\bar{p}^2 \bar{p}^2 \ln \left[1 - \frac{(G N_{\mathrm{c}} \Lambda^2)}{(8\pi^2)} \mathcal{J}_H(\bar{p}^2, \varepsilon^2) \right] \equiv V_{\mathrm{eff}}^{(\mathrm{ntl})} \ . \tag{C.10}$$

Therefore, we can really interpret the $V_{\mathrm{eff}}^{(\mathrm{ntl})}$ of (21) diagrammatically as the contribution of all those diagrams beyond the one loop which are next-to-leading order in the formal $1/N_{\mathrm{c}}$-expansion, provided $(G N_{\mathrm{c}} \Lambda^2)/(8\pi^2) = \mathcal{O}(1)$ as suggested by the 1-loop gap equation (24). On the other hand, the $V_{\mathrm{eff}}^{(\mathrm{ntl})}$ in eq. (21) was derived there by path integral method as the contribution of the *quadratic* fluctuations $\sigma_1(\bar{x})^2$ (cf. eq. (10)) of the Higgs field around its "classical" value H_0.

By arguments very similar to those at the beginning of this Appendix, we can demonstrate that the dominant (in the $1/N_{\mathrm{c}}$-expansion) 1-PI diagrams contributing to the mass renormalization of m_t are those of Figs. 5a-c - these are all the 1-PI diagrams of order $1/N_{\mathrm{c}}$ with two top quark outer legs. However, unlike the diagrams in Figs. 2-4, this time the top quark propagators in the loops have the non-zero *bare* mass m_t $(= m_t(\Lambda))$ - i.e., the mass obtained from the gap equation (34) (cf. Table 1, fifth column, or third column when QCD effects included). These graphs lead to the corrected propagator

$$D_t(q) = \frac{i}{\not{q} - m_t - \tilde{\pi}_t(\not{q}) + i\epsilon} \ , \qquad \tilde{\pi}_t(\not{q}) = \sum_{\ell=0}^{\infty} \tilde{\pi}_t^{(\ell+1)}(\not{q}) \ , \qquad m_t^{\mathrm{ren.}} = m_t + \tilde{\pi}(\not{q})|_{\not{q}=m_t} \ . \tag{C.11}$$

With $\tilde{\pi}_t^{(\ell+1)}(\not{q})$ we denote the contribution of the $(\ell+1)$-loop 1-PI diagram of Figs. 5, i.e., the one containing ℓ top quark loops with bare mass m_t. Using an approach similar to the one employed earlier in this Appendix for deriving the Green functions $\tilde{\Gamma}_H^{(2m;\ell+1)}$, and again carefully counting the number of possible contractions of H and $\bar{t}t$ (in the formalism of the Wick theorem), we obtain

$$\tilde{\pi}_t^{(\ell+1)}(\bar{\not{q}}) = (-1) \frac{1}{N_{\mathrm{c}}} \left(\frac{G N_{\mathrm{c}}}{2} \right) \int_{\bar{p}^2 \leq \Lambda^2} \frac{d^4 \bar{p}}{(2\pi)^4} [2 G N_{\mathrm{c}} \mathcal{K}_H(\bar{p}^2, m_t^2)]^{\ell} \frac{(\bar{\not{p}} + \bar{\not{q}} + m_t)}{[(\bar{p} + \bar{q})^2 + m_t^2]} \ , \tag{C.12}$$

where we used again the Euclidean metric with the simple spherical cut-off, and the notation (20) for the function $\mathcal{K}_H$. Summing up all these contributions, rescaling the momentum $\bar{p} \mapsto \Lambda \bar{p}$, and using the notations of (22) and (24), we arrive at

$$\frac{\tilde{\pi}_t(\bar{\not{q}})}{\Lambda} = \frac{(-1)}{N_{\rm c}} 4\pi^2 a \int_{\bar{p}^2 \leq 1} \frac{d^4\bar{p}}{(2\pi)^4} \frac{1}{[1 - a\mathcal{J}_H(\bar{p}^2, (m_t/\Lambda)^2)]} \frac{[\bar{\not{p}} + (\bar{\not{q}}/\Lambda) + (m_t/\Lambda)]}{[(\bar{p} + (\bar{q}/\Lambda))^2 + (m_t/\Lambda)^2]} \ . \tag{C.13}$$

The angular integration in this expression can be performed in a straightforward way by using 4-dimensional spherical coordinates in the coordinate system in which $\bar{q} = (0,0,0,|\bar{q}|)$ ($\Rightarrow \bar{p} \cdot \bar{q} = |\bar{p}||\bar{q}|\cos\theta$; $\bar{\not{q}} = \bar{\gamma}^3|\bar{q}|$) and the integral (B.2). After performing the angular integrations in (C.13), we are left with radial integration alone

$$\begin{aligned} \left.\frac{\tilde{\pi}_t(\bar{\not{q}})}{\Lambda}\right|_{\bar{\not{q}}=m_t} \quad = \quad & \frac{1}{4N_{\rm c}} a \int_0^1 \frac{d|\bar{p}|}{[1 - a\mathcal{J}_H(|\bar{p}|^2, x^2)]} \Big[\frac{1}{2x^3} |\bar{p}|^3 \left(|\bar{p}|^2 + 2x^2 - |\bar{p}|\sqrt{(|\bar{p}|^2 + 4x^2)} \right) + \\ & + \frac{2}{x}|\bar{p}|^2 \left(|\bar{p}| - \sqrt{(|\bar{p}|^2 + 4x^2)} \right) \Big] \ , \end{aligned} \tag{C.14}$$

where $x = (m_t/\Lambda)$, and we took into account the on-shell condition ($\bar{\not{q}} = \not{q} = m_t$, $\bar{q}^2 = -q^2 = -m_t^2$). This gives us the renormalized mass $m_t^{\rm ren.}$ in eq. (39), according to (C.11) - when we ignore the QCD effects.

The inclusion of the leading (i.e., 1-loop) QCD effects to the renormalization of m_t can be obtained from the diagram of Fig. 5a, where the dotted line now represents the gluon. This effect is well-known in the literature. It results in the following expression

$$(\delta m_t)^{\rm QCD}_{\alpha\beta} = -i\frac{g_{\rm s}^2}{4} \sum_{a,\gamma} \lambda^a_{\alpha\gamma}\lambda^a_{\gamma\beta} \int \frac{d^4p}{(2\pi)^4} \Big\{ \gamma^\mu \frac{i}{(\not{q} - \not{p} - m_t)} \gamma^\nu \frac{(-i)}{p^2} \left[g_{\mu\nu} - (1-\xi)\frac{p_\mu p_\nu}{p^2} \right] \Big\} \ , \tag{C.15}$$

where α and β are the color indices of the top quark, $\lambda^a/2$ are the $SU(3)_c$-generators, $g_{\rm s}$ is the QCD gauge coupling ($\alpha_{\rm s} = g_{\rm s}^2/(4\pi)$), and the top quark is taken on-shell ($\not{q} = m_t$). It turns out that the gauge-dependent part of the gluon propagator (proportional to $(1-\xi)$) does not contribute to $(\delta m_t)^{\rm QCD}$. Using the know relation of QCD

$$\sum_{a,\gamma} \lambda^a_{\alpha\gamma}\lambda^a_{\gamma\beta} = \frac{2(N_{\rm c}^2 - 1)}{N_{\rm c}}\delta_{\alpha\beta} \ ,$$

and the well-known techniques of rewriting the denominators as integrals of exponentials, we end up after some algebraic manipulations with the following (1-loop) result

$$(\delta m_t)^{\rm QCD}_{\alpha\beta} = \delta_{\alpha\beta}\frac{g_{\rm s}^2(N_{\rm c}^2 - 1)}{16\pi^2 N_{\rm c}} m_t \int_0^1 dz(1+z) \int_0^\infty \frac{d\tau}{\tau}\rho_{\rm f}(\tau, \Lambda_{\rm f}) \exp\left(-m_t^2 z\tau\right) \ . \tag{C.16}$$

Here we inserted the usual regulator $\rho_{\rm f}(\tau, \Lambda_{\rm f})$ to make the integral finite. For example, $\rho_{\rm f}$ may mean that we make a simple Pauli-Villars subtraction (with mass $\Lambda_{\rm f}$ replacing m_t). We can also choose the usual "proper-time" cut-off: $\rho_{\rm f} = 0$ for $\tau < 1/\Lambda_{\rm f}^2$, and $\rho_{\rm f} = 1$ otherwise. In the results of this paper, we have, for simplicity, always equated the cut-offs for the quark and the bosonic momenta: $\Lambda_{\rm f} = \Lambda_{\rm b} = \Lambda$.

References

[1] Y. Nambu and G. Jona-Lasinio, Phys. Rev. **122**, 345 (1961).

[2] Y. Nambu, Proceedings of the Kazimierz Conference "New Theories in Physics" (1988), pp. 1-10.

[3] V. A. Miranski, M. Tanabashi and K. Yamawaki, Mod. Phys. Lett. A **4**, 1043 (1989); Phys. Lett. B **221**, 177 (1989).

[4] W. A. Bardeen, C. T. Hill and M. Lindner, Phys. Rev. D **41**, 1647 (1990).

[5] A. King and S. H. Mannan, Phys. Lett. B **241**, 249 (1990); C. T. Hill, M. A. Luty and E. A. Paschos, Phys. Rev. D **43**, 3011 (1991); Y. Achiman and A. Davidson, Phys. Lett. B **261**, 431 (1991); A. Hasenfratz, P. Hasenfratz, K. Jansen, J. Kuti and Y. Shen, Nucl. Phys. **B365**, 79 (1991).

[6] M. Suzuki, Phys. Rev. D **41**, 3457 (1990); M. Harada and N. Kitazawa, Phys. Lett. B **257**, 383 (1991).

[7] J.M. Cornwall, R. Jackiw and E. Tomboulis, Phys. Rev. D **10**, 2428 (1974).

[8] K. Higashijima, Prog. Theor. Phys. Supp. **104** (1991).

[9] R. Fukuda and E. Kyriakopoulos, Nucl. Phys. **B85**, 354 (1975).

[10] G. Cvetič and E.A. Paschos, Nucl. Phys. **B395**, 581 (1993).

[11] D. Bailin and A. Love, *Introduction to Gauge Field Theory* (Adam Hilger, Bristol and Boston, 1986).

[12] H.D. Politzer, Nucl. Phys. **B117**, 397 (1976).

[13] CDF Collaboration, F. Abe *et al.*, Phys. Rev. Lett. **72**, 225 (1994); also preprint FERMILAB-PUB-95-149-E (hep-ex/9506006).

[14] S. Hands, A. Kocić and J.B. Kogut, Phys. Lett. B **273**, 111 (1991).

[15] A. Blumhofer, Nucl. Phys. **B437**, 25 (1995).

[16] T. Gherghetta, Phys. Rev. D **50**, 5985 (1994).

Table 1

$a=\frac{N_{\rm c}G\Lambda^2}{8\pi^2}$	$\sqrt{z_1}=\frac{m_t^{(1)}}{\Lambda}$	$\sqrt{z}=\frac{m_t^{(H+gl)}}{\Lambda}$	$\frac{\left(m_t^{(H+gl)}\right)^{\rm ren.}}{\Lambda}$	$\frac{m_t^{(H)}}{\Lambda}$	$\frac{\left(m_t^{(H)}\right)^{\rm ren.}}{\Lambda}$
2.198	0.70	0.669	0.575	0.657	0.532
1.918	0.60	0.555	0.477	0.538	0.429
1.673	0.50	0.432	0.368	0.399	0.303
1.605	0.469	0.389	0.328	0.332	0.237
1.5970	0.46543	0.384	0.323	0.309	0.213
1.5969	0.4654	0.384	0.323	-	-
1.564	0.45	0.359	0.300	-	-
1.523	0.43	0.321	0.264	-	-
1.506	0.4215	0.299	0.241	-	-
1.503	0.42	0.293	0.235	-	-
1.4988	0.41785	0.277	0.217	-	-
1.4987	0.4178	-	-	-	-

4 Table and figure captions

Table 1: The solutions $\sqrt{z} = (m_t/\Lambda)$ (3rd column) of the improved gap equation (34), for a given input $a = (N_{\rm c} G \Lambda^2)/(8\pi^2)$ (1st column), where G is the 4-fermion coupling of the TSM (see (1)) and Λ is the upper energy cut-off (i.e., roughly the energy at which the condensation takes place). The last entry in a column corresponds to the disappearance of the non-trivial minimum. The 4th column contains the corresponding renormalized top quark masses. The 5th and the 6th columns contain the solutions (m_t/Λ) and their renormalized values, respectively, for the case when the QCD effects are ignored. $N_{\rm c} = 3$ was taken.

Figs. 1(a)-1(e): Effective potential $V_{\rm eff}$ as function of $\varepsilon^2 = H_0^2 (G M_0^2)/(2\Lambda^2)$. For convenience, $V_{\rm eff}$ is multiplied by $\chi = 8\pi^2/(N_{\rm c}\Lambda^4)$. The notation "ntl(H+gluons)" means that all the next-to-leading $1/N_{\rm c}$-contributions of the Higgs sector and the dominant part of the QCD contributions are included; "ntl(H)" means the same, but without QCD. Where possible, we also included the curves for the case of (0+1+2)-loop (without QCD) and (0+1)-loop calculation. We took $N_{\rm c} = 3$ and the input values $a = (N_{\rm c} G \Lambda^2)/(8\pi^2) \simeq 2.198$, 1.673, 1.564, 1.5031, 1.4982, respectively (corresponding to the 1-loop minima $\sqrt{z_1} = m_t^{(1)}/\Lambda = 0.7$, 0.5, 0.45, 0.42, 0.4175, respectively).

Figs. 2(a)-(c): The 1-loop 1-PI diagrams contributing to 1-PI Green functions $\tilde{\Gamma}_H^{(2m;1)}(p_1, \ldots, p_{2m})$; incidentally, they give at the same time the leading order terms in the formal $1/N_{\rm c}$-expansion of $V_{\rm eff}$ (of order $\mathcal{O}(N_{\rm c})$). Full lines represent massless top quarks, and dotted lines the scalar non-dynamical Higgs of the Lagrangian (2) (same notation also in Figs. 4, 5, 6).

Fig. 3: The $(\ell + 1)$-loop 1-PI diagrams which contribute to the 1-PI Green functions $\tilde{\Gamma}_H^{(2m;\ell+1)}(p_1, \ldots, p_{2m})|_{\{p_k\}=\{0\}}$ and which yield the next-to-leading order terms (beyond 1-loop) in the formal $1/N_{\rm c}$-expansion of $V_{\rm eff}$ (of order $\mathcal{O}((GN_{\rm c})^\ell) = \mathcal{O}(1)$). The diagrams contain ℓ loops of (massless) top quarks. These loops are connected into another circle by ℓ propagators of the (non-dynamical) Higgs. The j^{th} fermionic loop ($j = 1, \ldots, \ell$) has $(2m_j)$ outer legs of Higgses with zero momenta attached to it (n_j and $(2m_j - n_j)$ on the "outer" and the "inner" halves, respectively). The total number of outer legs with zero momenta is $2(m_1 + \cdots + m_\ell) = 2m$.

Figs. 4(a)-(b): Examples of 3-loop and 4-loop 1-PI diagrams which, while in principle contributing to $\tilde{\Gamma}_H^{(2m;3)}(p_1, \ldots, p_{2m})$, do not contribute to the next-to-leading order terms ($\mathcal{O}(1)$) of V_{eff} in the formal $1/N_{\text{c}}$-expansion, but rather to terms $\mathcal{O}(G^2 N_{\text{c}}) = \mathcal{O}(G^3 N_{\text{c}}^2) = \mathcal{O}(1/N_{\text{c}})$. This is so because the colors of all the (massless) top quarks in a given quark loop are forced to be equal and the number of quark loops is smaller than that in the 3-loop and 4-loop diagrams of Fig. 3, respectively.

Figs. 5(a)-(c): the 1-PI diagrams with two outer top quark legs which give the leading ($\mathcal{O}(1/N_{\text{c}})$) contribution to the renormalization of the mass m_t. Unlike the diagrams of Figs. 2-4, the top quark propagators here contain the non-zero bare mass m_t which was the solution to the gap equation in the next-to-leading order in $1/N_{\text{c}}$.

Fig.1a

$a=2.198\ (m^{(1)}/\Lambda)=0.7$

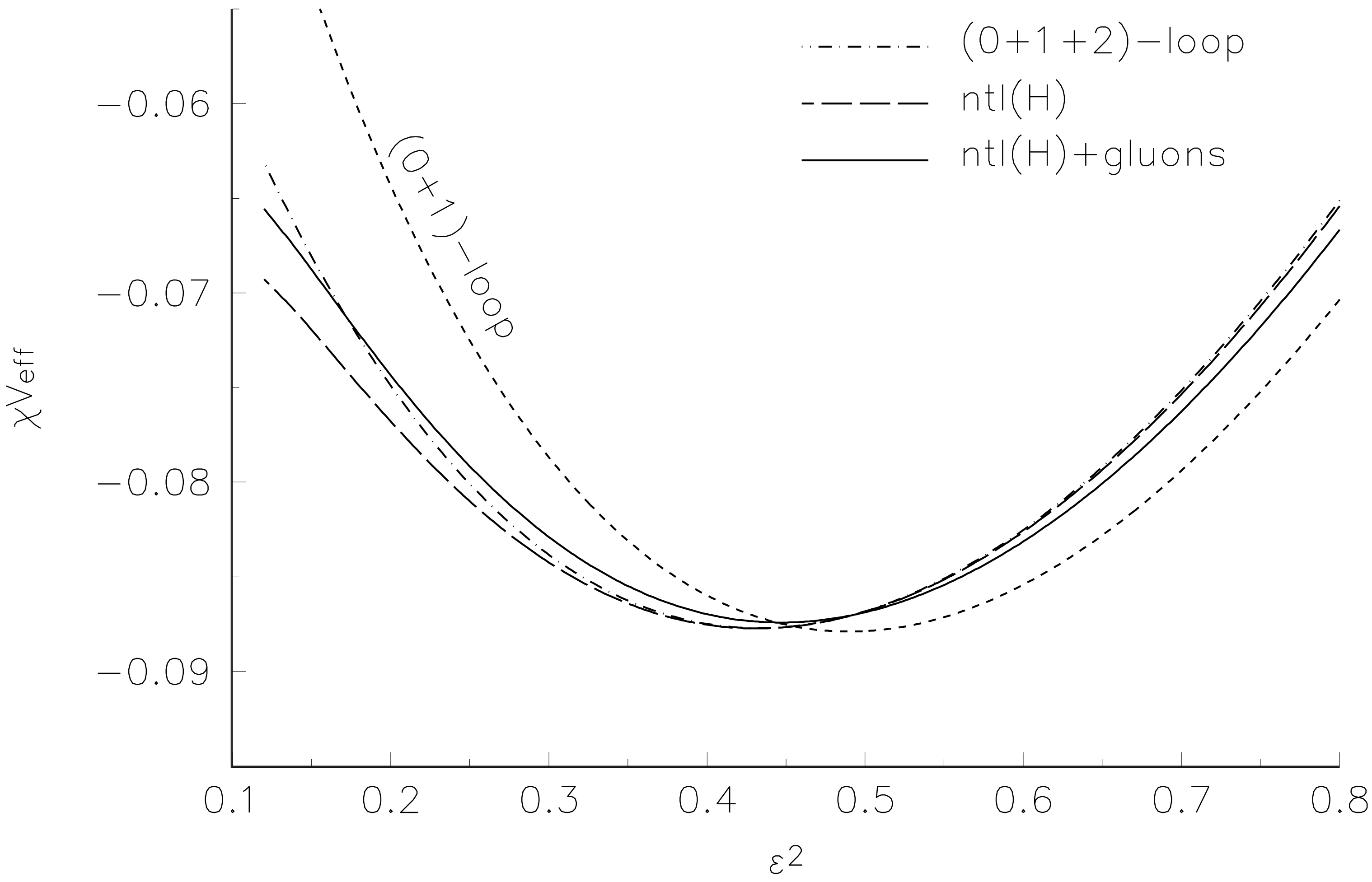

Fig.1b

$a=1.673\ (m^{(1)}/\Lambda) = 0.5$

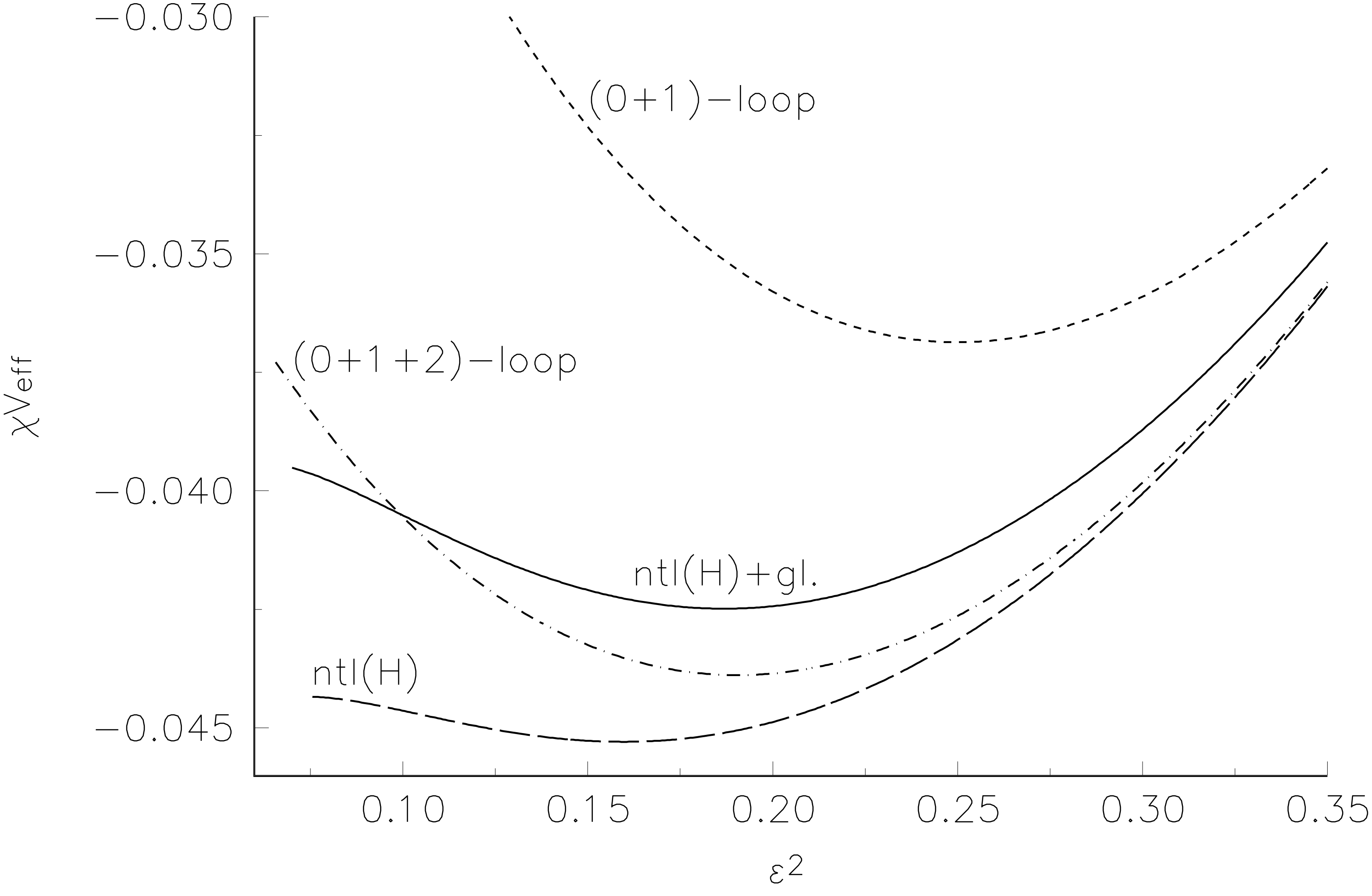

Fig.1 c

$a=1.564\ ((m^{(1)}/\Lambda)=0.45)$

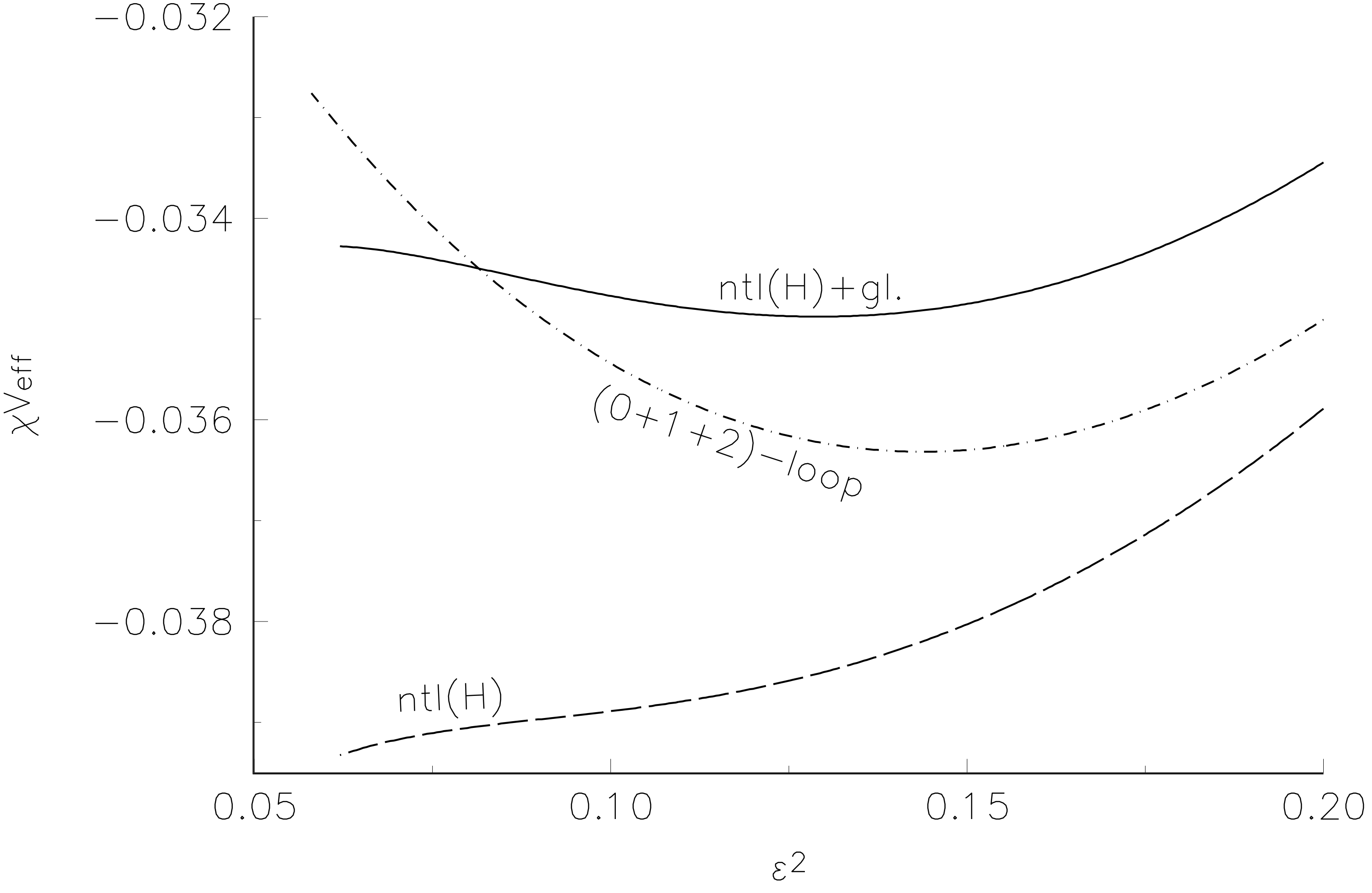

Fig.1d

$a=1.5031\ ((m^{(1)}/\Lambda)=0.42)$

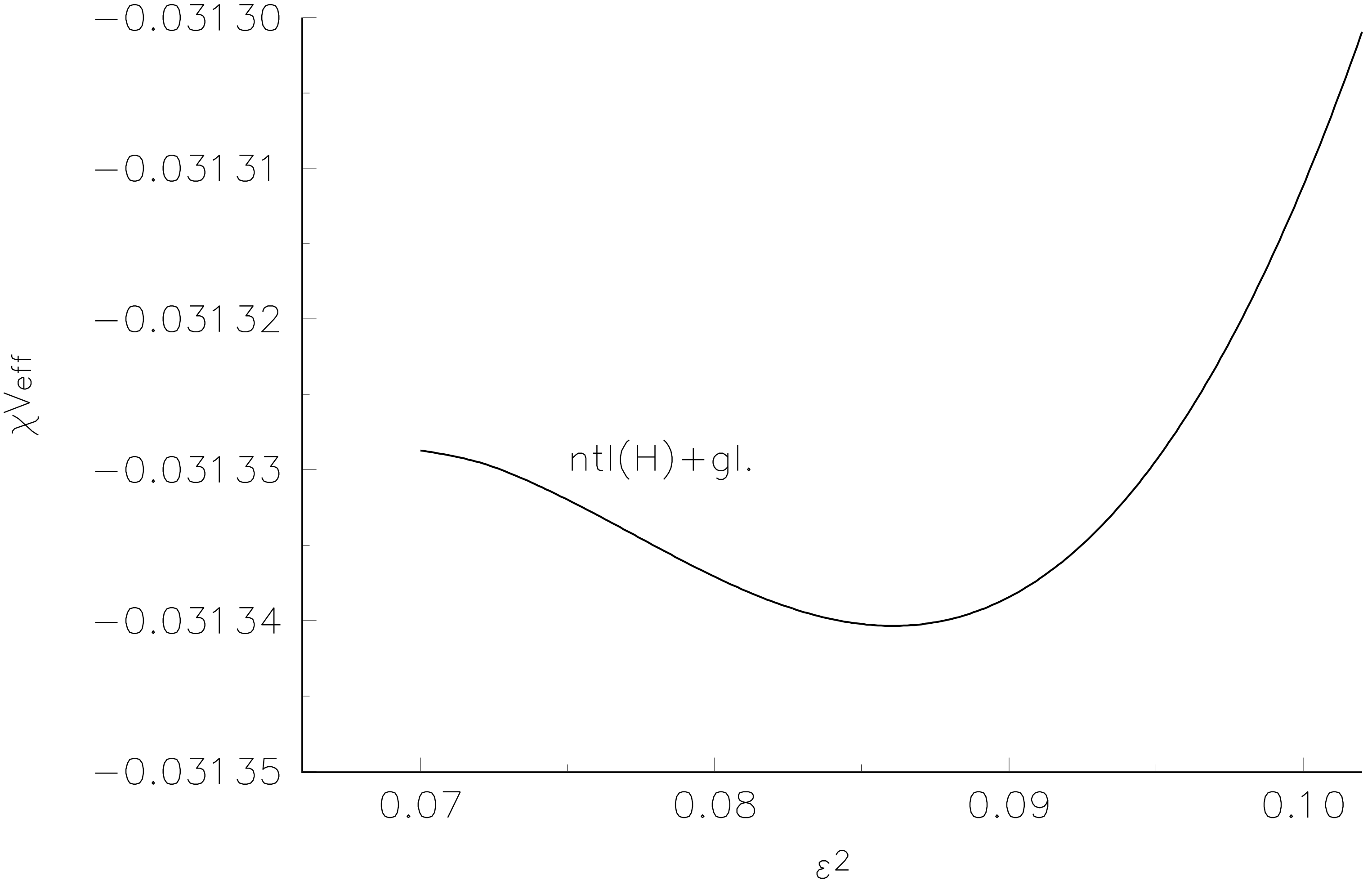

Fig.1e

$a=1.4982$ $((m^{(1)}/\Lambda)=0.4175)$

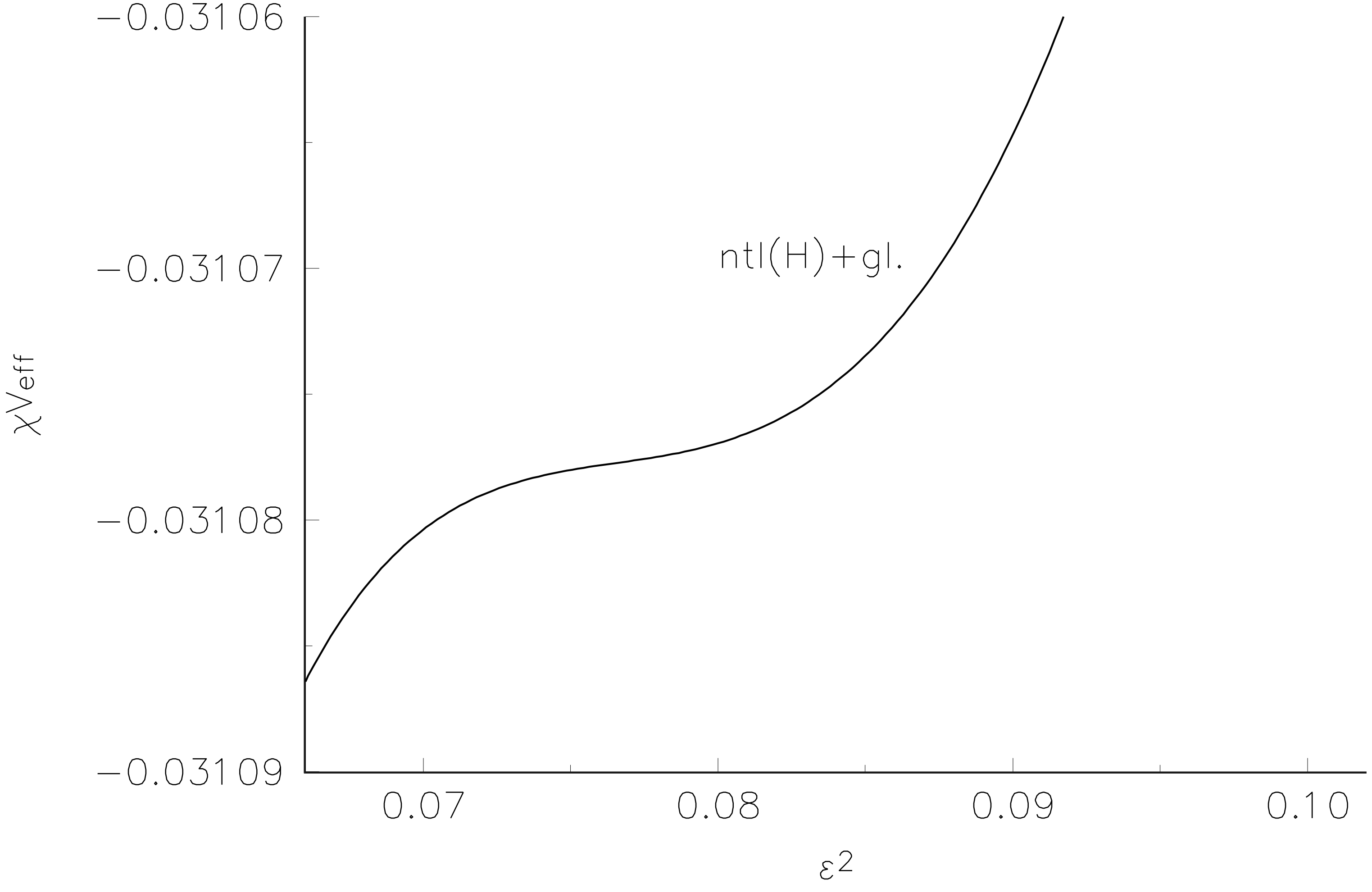

This figure "fig1-1.png" is available in "png" format from:

http://arXiv.org/ps/hep-ph/9501268v2

This figure "fig2-1.png" is available in "png" format from:

http://arXiv.org/ps/hep-ph/9501268v2

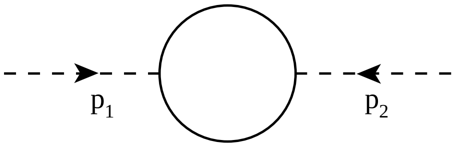

Fig. 2a

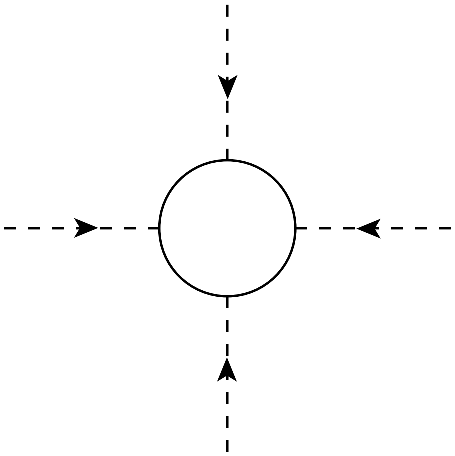

Fig. 2b

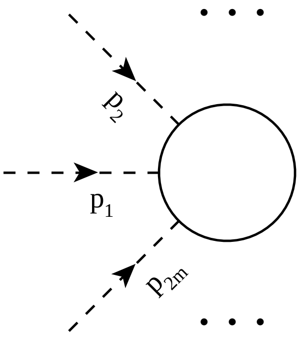

Fig. 2c

This figure "fig1-2.png" is available in "png" format from:

http://arXiv.org/ps/hep-ph/9501268v2

This figure "fig2-2.png" is available in "png" format from:

http://arXiv.org/ps/hep-ph/9501268v2

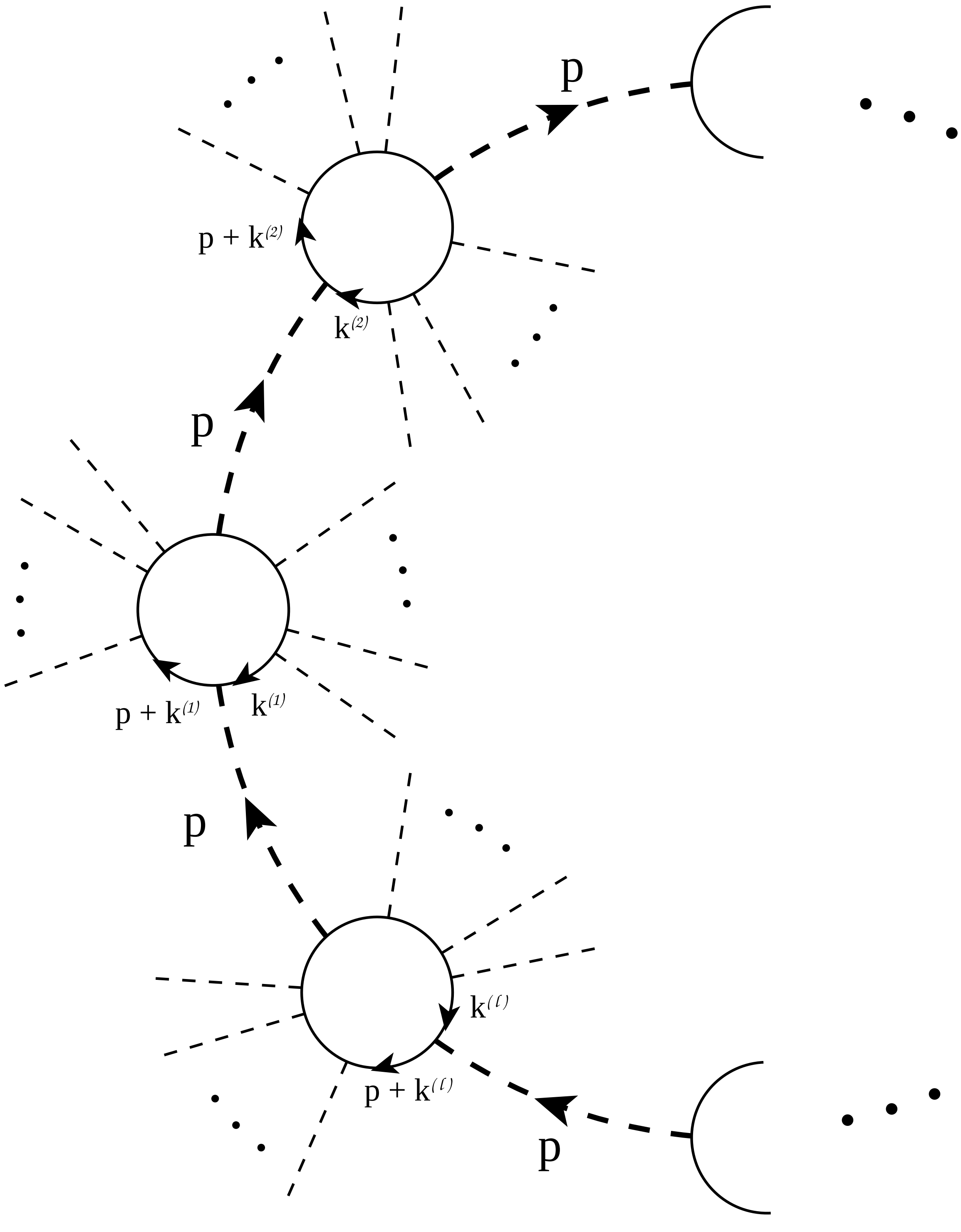

Fig. 3

This figure "fig1-3.png" is available in "png" format from:

http://arXiv.org/ps/hep-ph/9501268v2

This figure "fig2-3.png" is available in "png" format from:

http://arXiv.org/ps/hep-ph/9501268v2

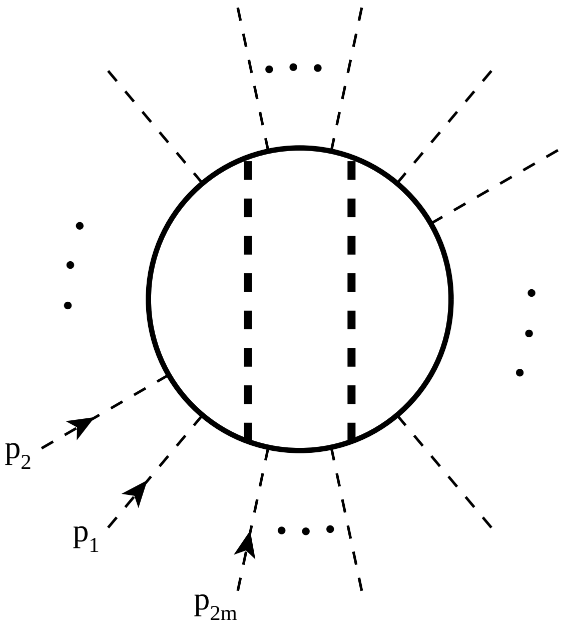

Fig. 4a

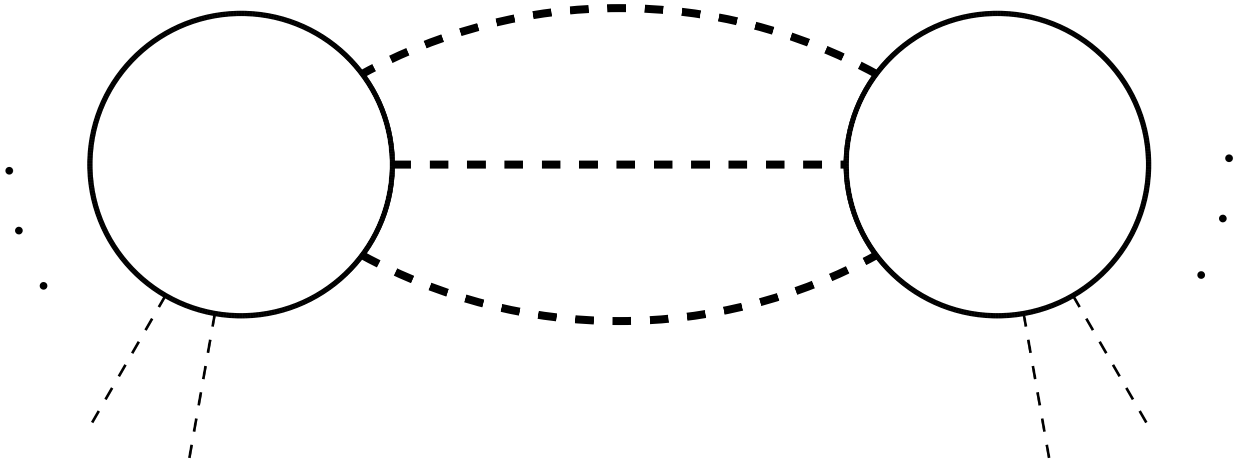

Fig. 4b

This figure "fig1-4.png" is available in "png" format from:

http://arXiv.org/ps/hep-ph/9501268v2

This figure "fig2-4.png" is available in "png" format from:

http://arXiv.org/ps/hep-ph/9501268v2

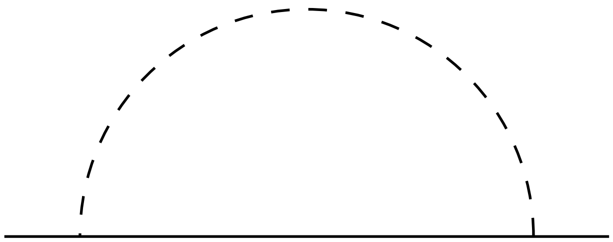

Fig. 5a

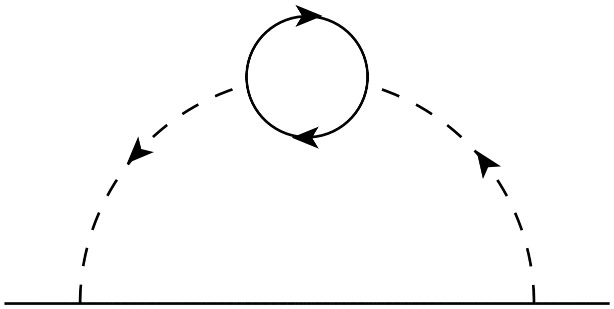

Fig. 5b

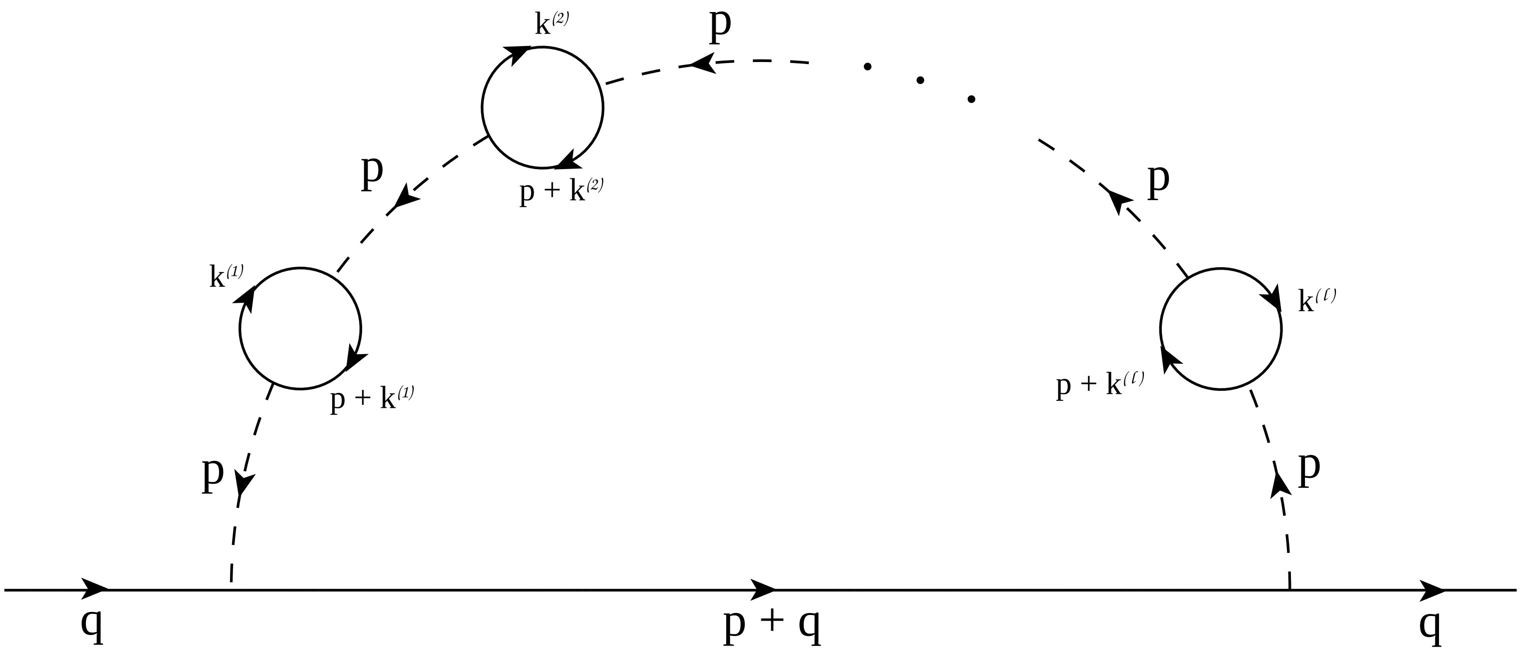

Fig. 5c

This figure "fig1-5.png" is available in "png" format from:

http://arXiv.org/ps/hep-ph/9501268v2

This figure "fig2-5.png" is available in "png" format from:

http://arXiv.org/ps/hep-ph/9501268v2